Klimaänderung II

4. Das zukünftige globale Klima: Szenarien-basierte Projektionen und kurzfristiger Ausblick

Robert Sausen

Institut für Physik der Atmosphäre
Deutsches Zentrum für Luft- und Raumfahrt
Oberpfaffenhofen

Vorlesung SS 2022

LMU München

Technical information

- http://www.pa.op.dlr.de/~RobertSausen/vorlesung/index.html
  - Most recent update on the lecture
  - Slides of the lecture (with some delay)

  - See also LSF https://lsf.verwaltung.uni-muenchen.de/

- Contact: robert.sausen@dlr.de

- Further information:
  - www.ipcc.ch
  - www.de-ipcc.de

Contents of IPCC AR 6 2021
Working Group I: the Physical Science Basis

Chapters

Chapter 1: Framing, context, methods	DOWNLOAD
Chapter 2: Changing state of the climate system	DOWNLOAD
Chapter 3: Human influence on the climate system	DOWNLOAD
Chapter 4: Future global climate: scenario-based projections and near-term information	DOWNLOAD
Chapter 5: Global carbon and other biogeochemical cycles and feedbacks	DOWNLOAD
Chapter 6: Short-lived climate forcers	DOWNLOAD
Chapter 7: The Earth's energy budget, climate feedbacks, and climate sensitivity	DOWNLOAD
Chapter 8: Water cycle changes	DOWNLOAD
Chapter 9: Ocean, cryosphere, and sea level change	DOWNLOAD
Chapter 10: Linking global to regional climate change	DOWNLOAD
Chapter 11: Weather and climate extreme events in a changing climate	DOWNLOAD
Chapter 12: Climate change information for regional impact and for risk assessment	DOWNLOAD
Atlas	DOWNLOAD

Supplementary Material

Annexes

https://www.ipcc.ch/report/ar6/wg1/#FullReport

Evaluation and communication of degree of certainty in AR6 findings

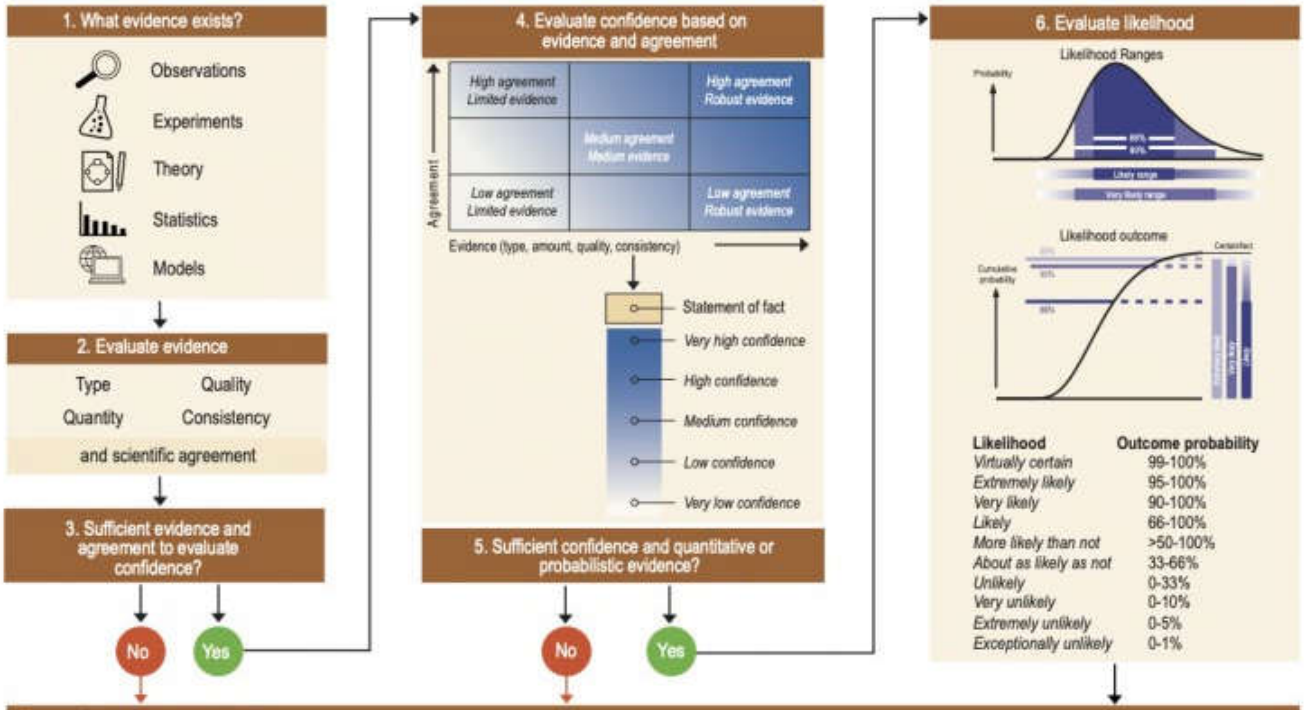

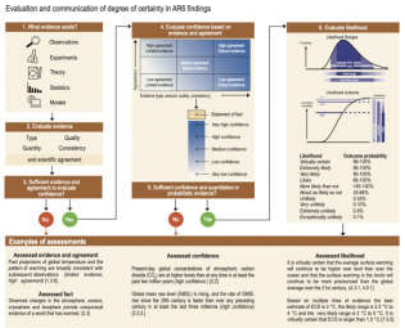

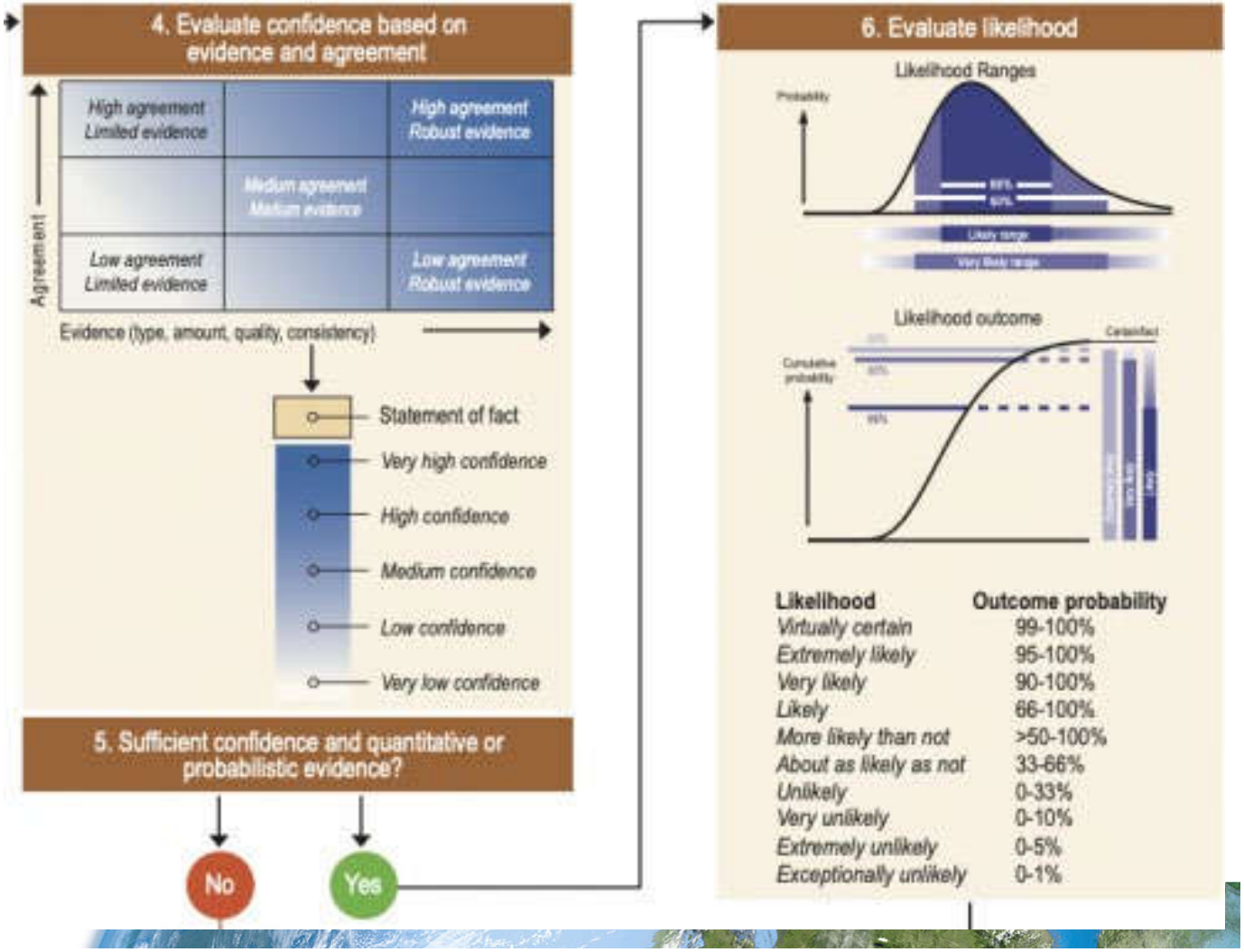

IPCC 2021, Chap. 1

Die SSP-Szenarien
Shared Socioeconomic Pathways

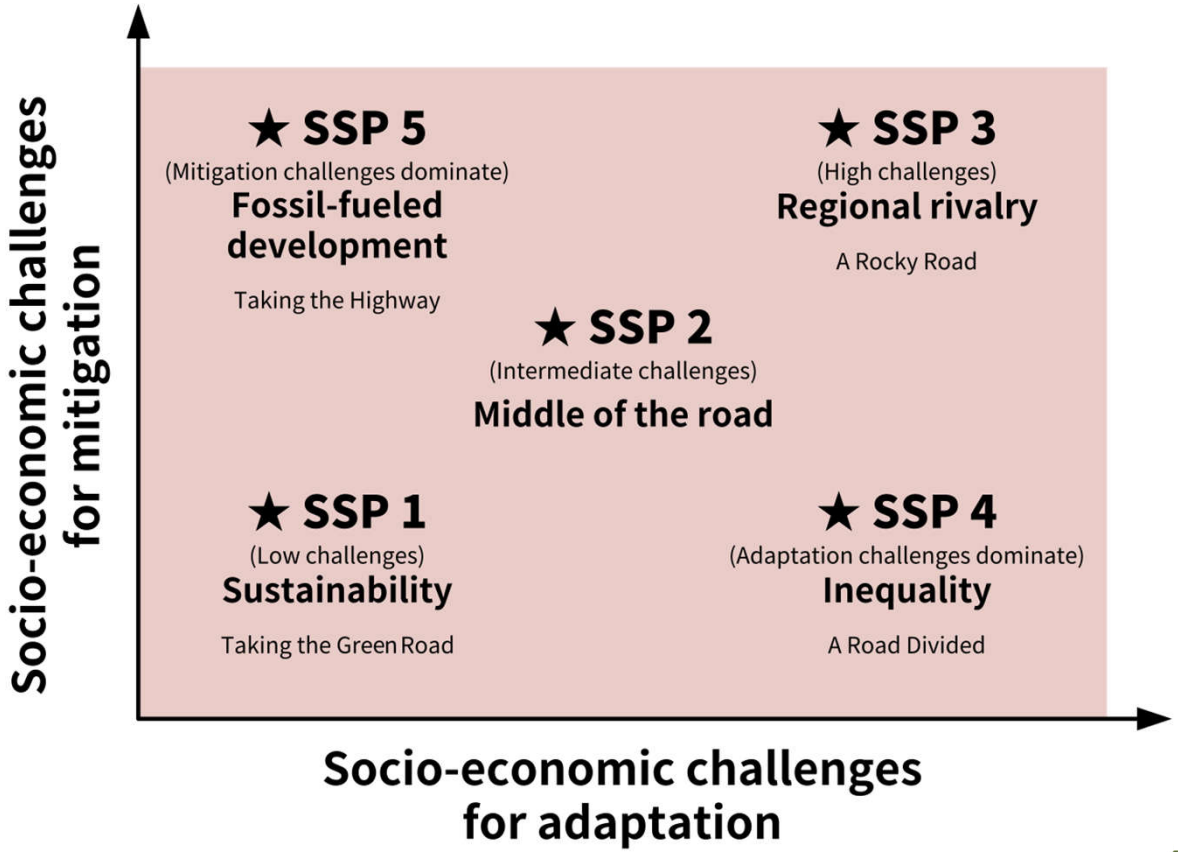

https://en.wikipedia.org

Die SSP-Szenarien – Shared Socioeconomic Pathways

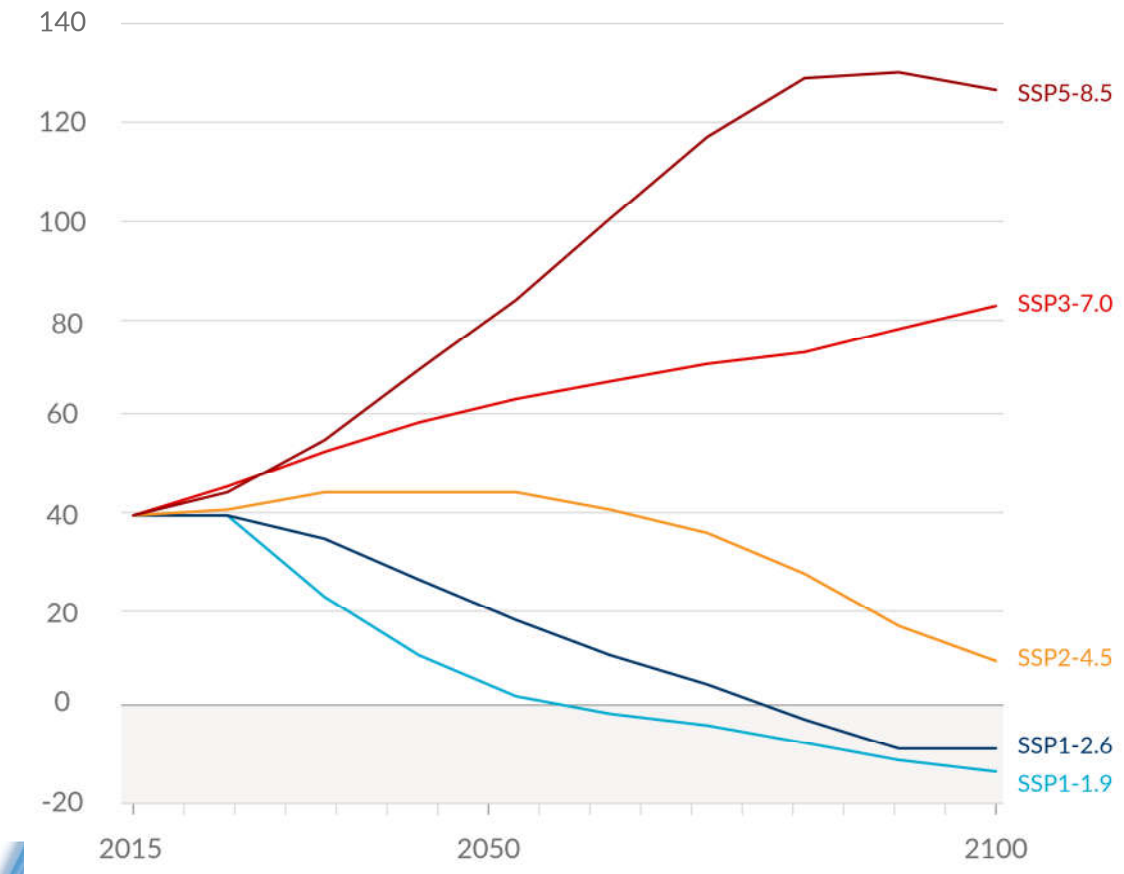

IPCC 2021, SPM

Selected indicators of global climate change from CMIP6 historical and scenario simulations

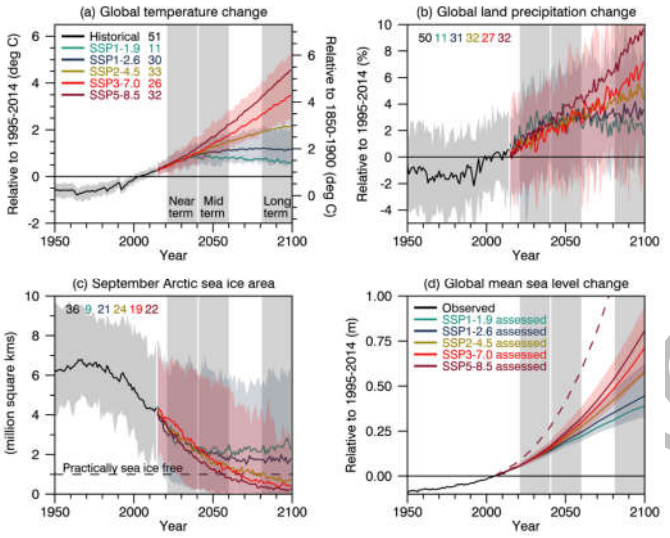

Figure 4.2: **Selected indicators of global climate change from CMIP6 historical and scenario simulations.** (a) Global surface air temperature changes relative to the 1995–2014 average (left axis) and relative to the 1850–1900 average (right axis; offset by 0.82°C, which is the multi-model mean and close to observed best estimate, Cross-Chapter Box 2.1, Table 1). (b) Global land precipitation changes relative to the 1995–2014 average. (c) September Arctic sea-ice area. (d) Global mean sea-level change (GMSL) relative to the 1995–2014 average. (a), (b) and (d) are annual averages, (c) are September averages. In (a)-(c), the curves show averages over the CMIP6 simulations, the shadings around the SSP1-2.6 and SSP3-7.0 curves show 5–95% ranges, and the numbers near the top show the number of model simulations used. Results are derived from concentration-driven simulations. In (d), the barystatic contribution to GMSL (i.e., the contribution from land-ice melt) has been added offline to the CMIP6 simulated contributions from thermal expansion (thermosteric). The shadings around the SSP1-2.6 and SSP3-7.0 curves show 5–95% ranges. The dashed curve is the *low confidence* and low likelihood outcome at the high end of SSP5-8.5 and reflects deep uncertainties arising from potential ice-sheet and ice-cliff instabilities. This curve at year 2100 indicates 1.7 m of GMSL rise relative to 1995–2014. More information on the calculation of GMSL are available in Chapter 9, and further regional details are provided in the Atlas. Further details on data sources and processing are available in the chapter data table (Table 4.SM.1).

IPCC 2021, Chap. 4

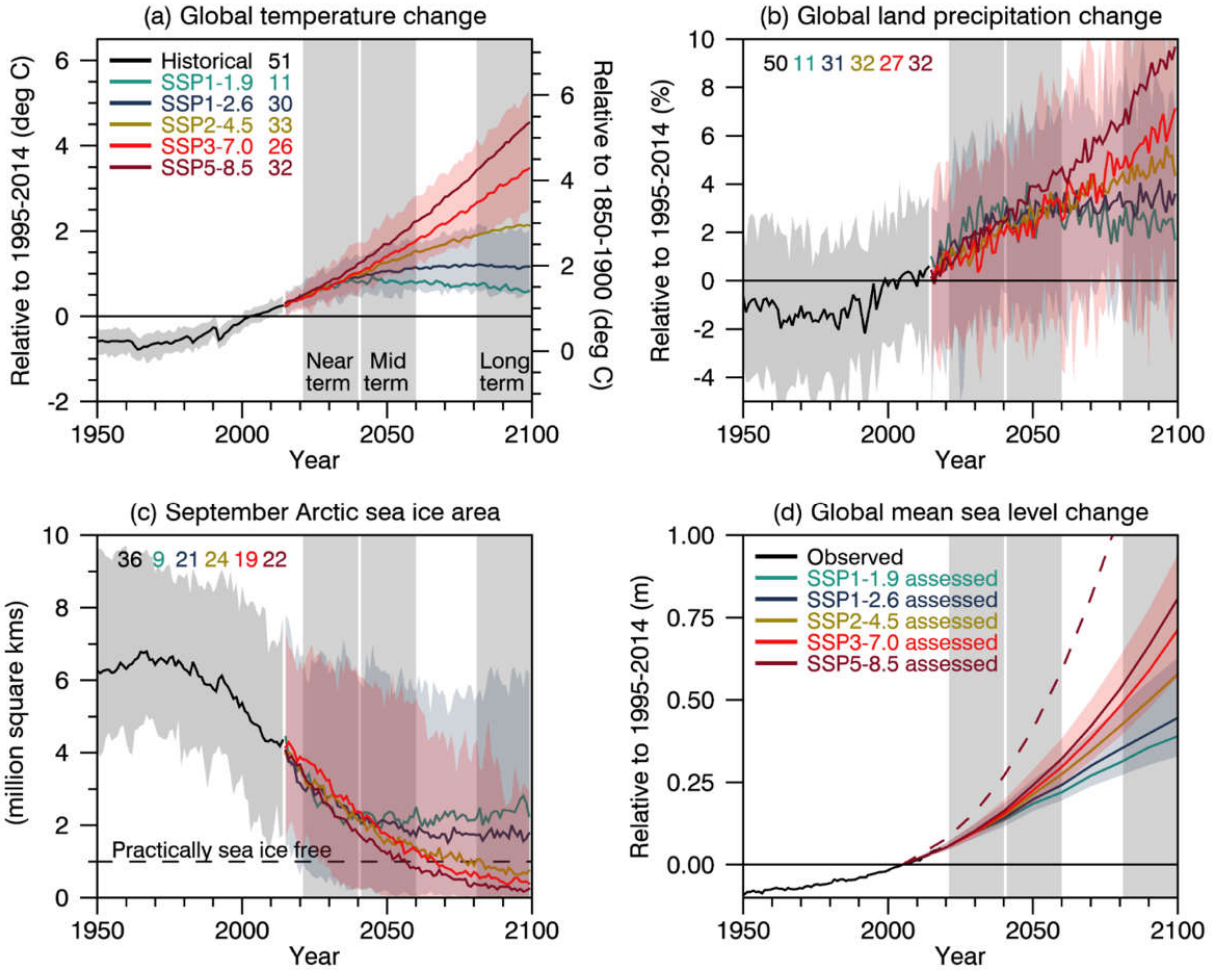

IPCC 2021, Chap. 4

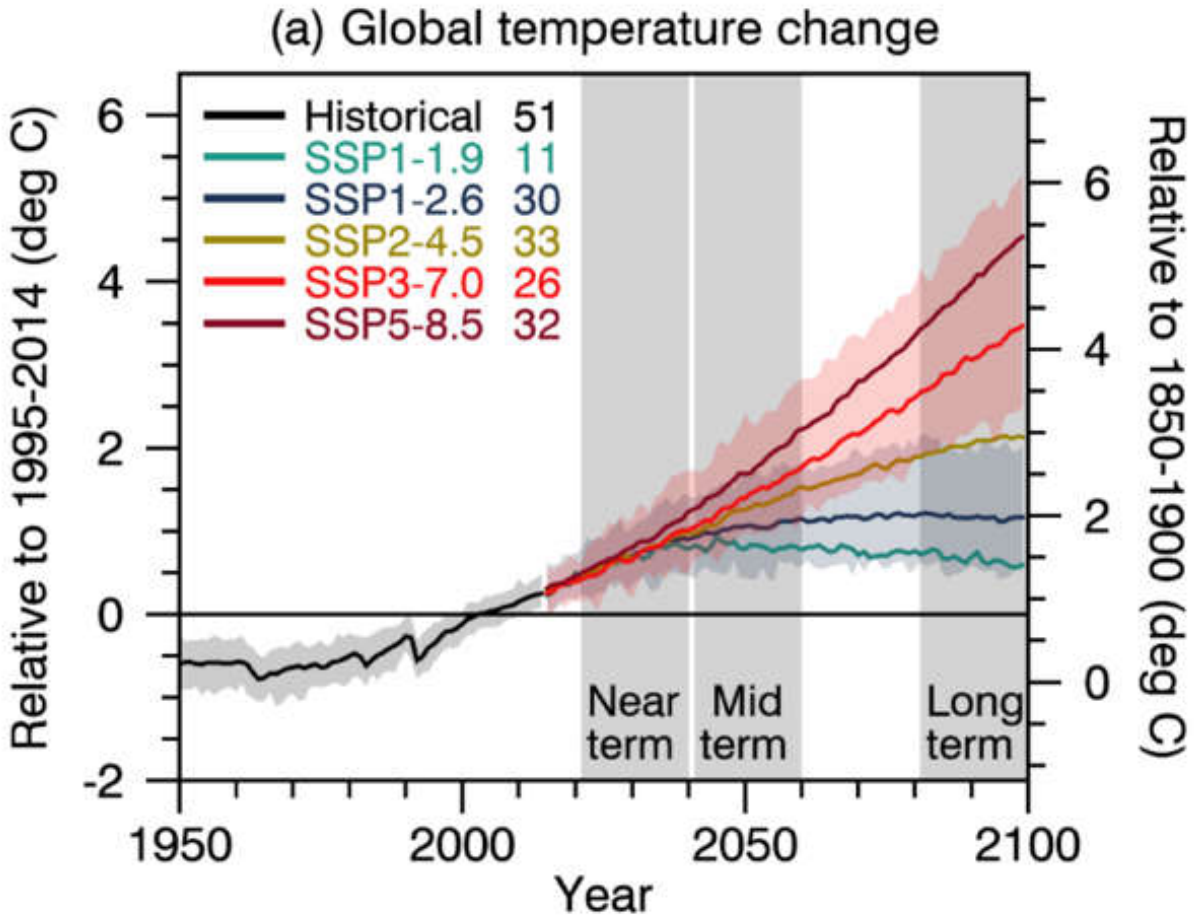

IPCC 2021, Chap. 4

Near-term change of seasonal mean surface temperature

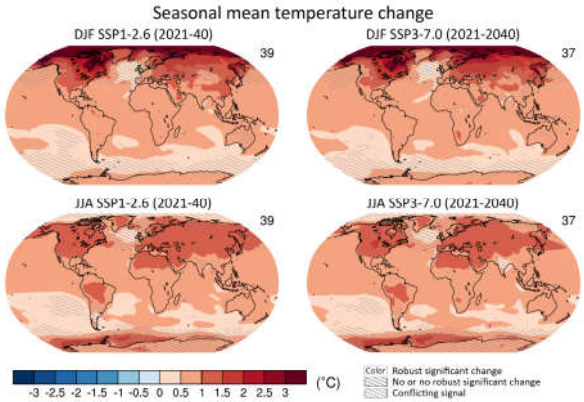

Figure 4.12: Near-term change of seasonal mean surface temperature. Displayed are projected spatial patterns of CMIP6 multi-model mean change (°C) in (top) DJF and (bottom) JJA near-surface air temperature for 2021–2040 from SSP1-2.6 and SSP3-7.0 relative to 1995–2014. The number of models used is indicated in the top right of the maps. No overlay indicates regions where the change is robust and *likely* emerges from internal variability, that is, where at least 66% of the models show a change greater than the internal-variability threshold (see Section 4.2.6) and at least 80% of the models agree on the sign of change. Diagonal lines indicate regions with no change or no robust significant change, where fewer than 66% of the models show change greater than the internal-variability threshold. Crossed lines indicate areas of conflicting signals where at least 66% of the models show change greater than the internal-variability threshold but fewer than 80% of all models agree on the sign of change. Further details on data sources and processing are available in the chapter data table (Table 4.SM.1).

IPCC 2021, Chap. 4

Seasonal mean temperature change

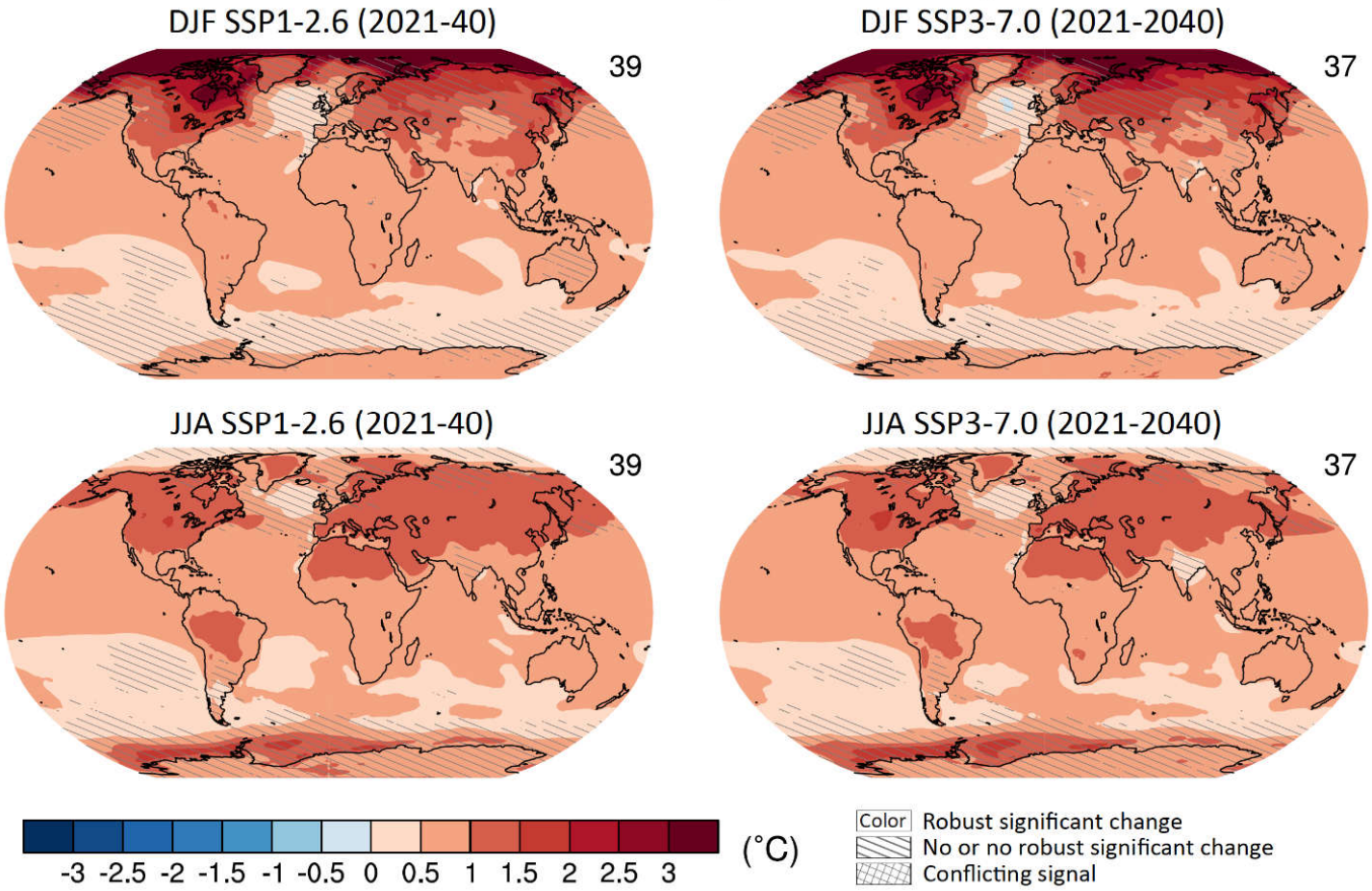

IPCC 2021, Chap. 4

Simulations over the period 1995–2040, encompassing the recent past and the next twenty years, of two important indicators of global climate change

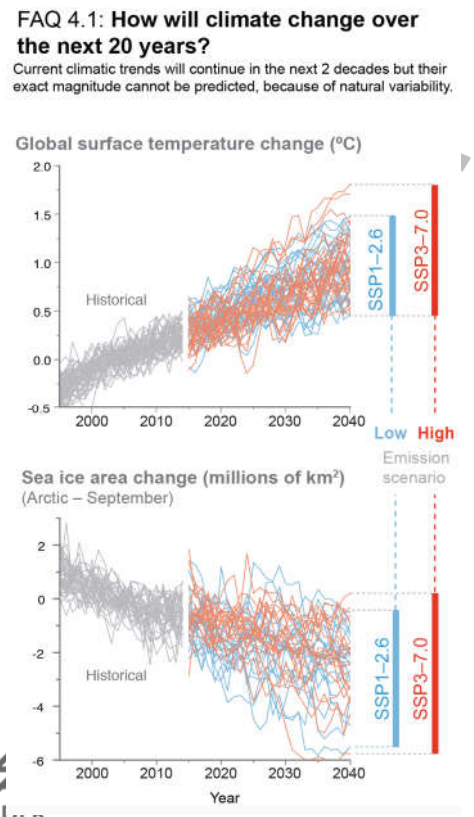

FAQ 4.1, Figure 1: Simulations over the period 1995–2040, encompassing the recent past and the next twenty years, of two important indicators of global climate change. (top) global surface temperature, and (bottom), the area of Arctic sea ice in September. Both quantities are shown as deviations from the average over the period 1995–2014. The black curves are for the historical period ending in 2014; the blue curves represent a low-emission scenario (SSP1-2.6) and the red curves one high-emission scenario (SSP3-7.0).

IPCC 2021, Chap. 4

FAQ 4.1: **How will climate change over the next 20 years?**

Current climatic trends will continue in the next 2 decades but their exact magnitude cannot be predicted, because of natural variability.

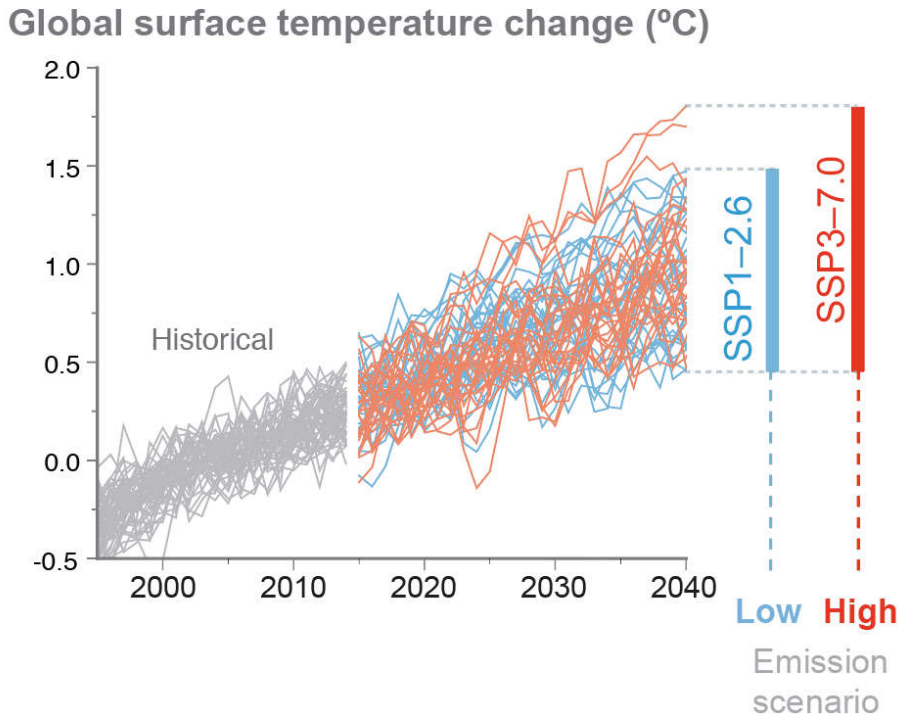

IPCC 2021, Chap. 4

Mid- and long-term change of annual mean surface temperature

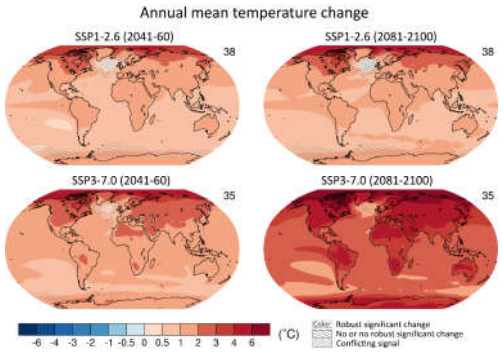

Figure 4.19: Mid- and long-term change of annual mean surface temperature. Displayed are projected spatial patterns of multi-model mean change in annual mean near-surface air temperature (°C) in 2041–2060 and 2081–2100 relative to 1995–2014 for (top) SSP1-2.6 and (bottom) SSP3-7.0. The number of models used is indicated in the top right of the maps. No overlay indicates regions where the change is robust and *likely* emerges from internal variability, that is, where at least 66% of the models show a change greater than the internal-variability threshold (see Section 4.2.6) and at least 80% of the models agree on the sign of change. Diagonal lines indicate regions with no change or no robust significant change, where fewer than 66% of the models show change greater than the internal-variability threshold. Crossed lines indicate areas of conflicting signals where at least 66% of the models show change greater than the internal-variability threshold but fewer than 80% of all models agree on the sign of change. Further details on data sources and processing are available in the chapter data table (Table 4.SM.1).

IPCC 2021, Chap. 4

Annual mean temperature change

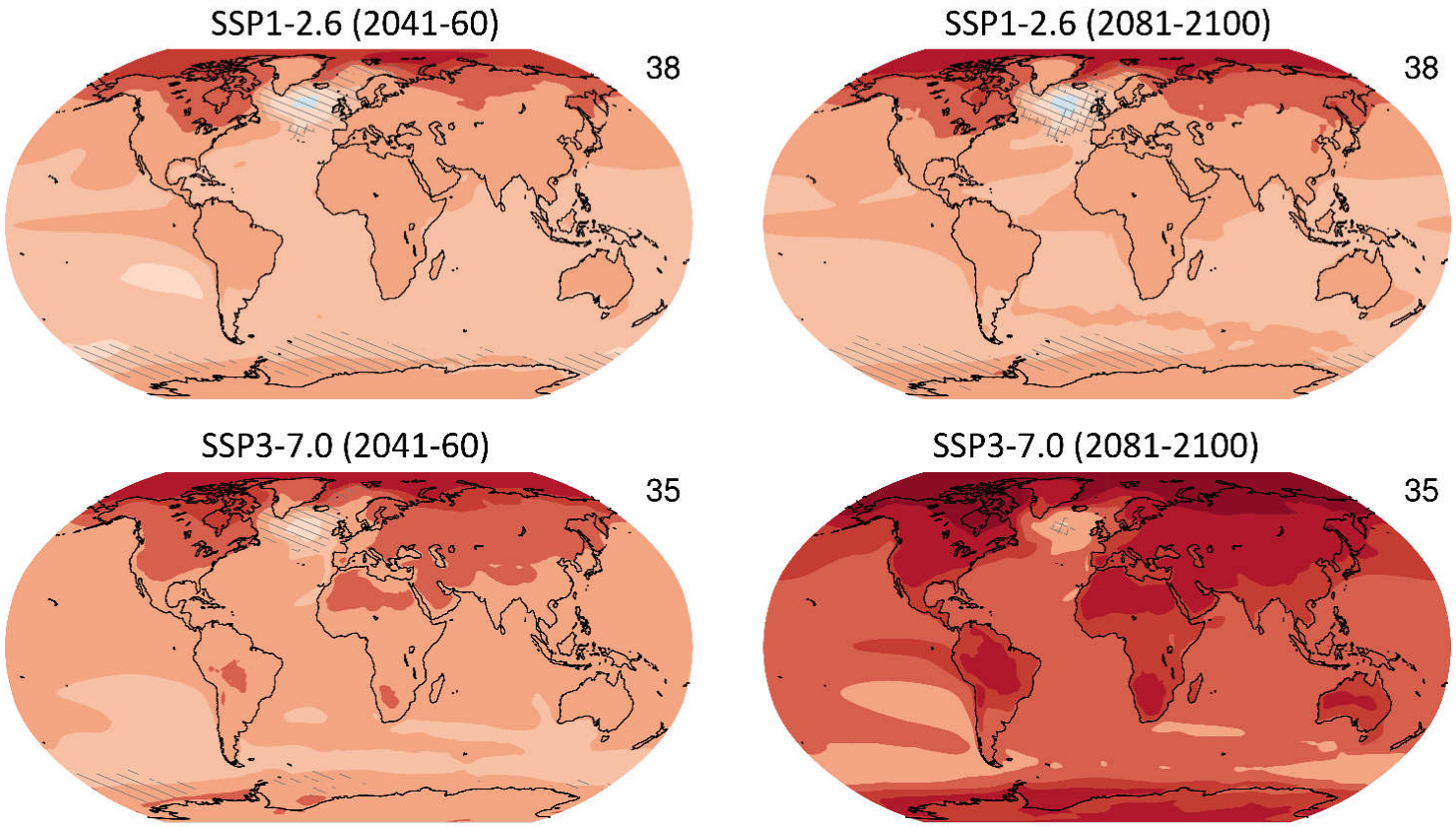

IPCC 2021, Chap. 4

Difference of surface temperature change between JJA and DJF

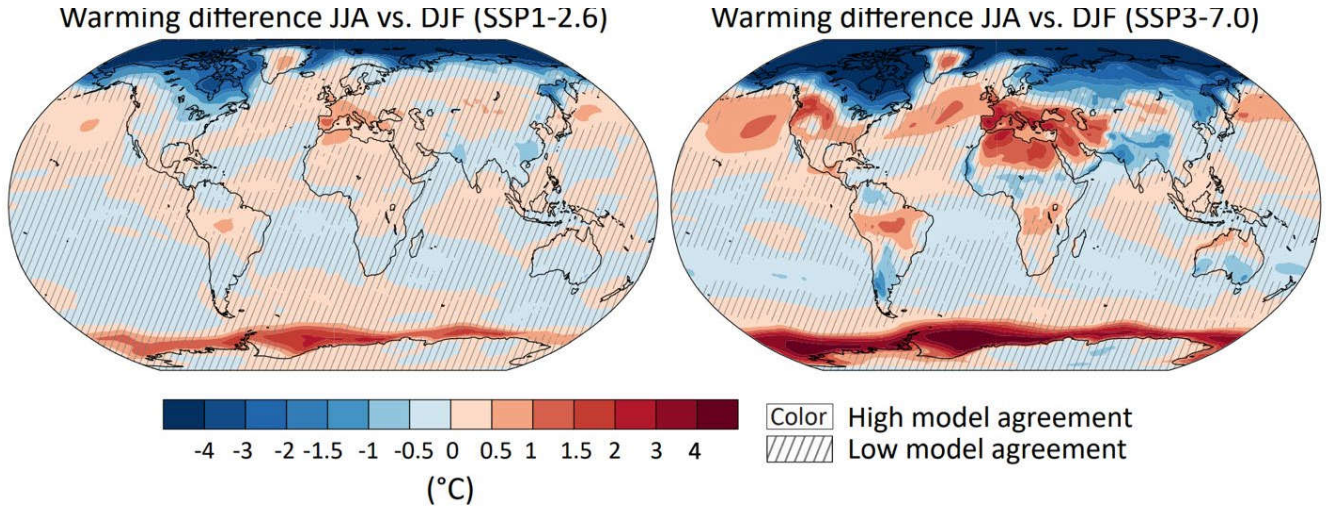

Figure 4.20: Difference of surface temperature change between JJA and DJF. Displayed are spatial patterns of multi-model mean difference in projected warming in JJA minus warming in DJF in 2081–2100 relative to 1995–2014 for (left) SSP1-2.6 and (right) SSP3-7.0. Diagonal lines mark areas where fewer than 80% of the models agree on the sign of change, and no overlay where at least 80% of the models agree. Further details on data sources and processing are available in the chapter data table (Table 4.SM.1).

IPCC 2021, Chap. 4

Difference of surface temperature change between JJA and DJF

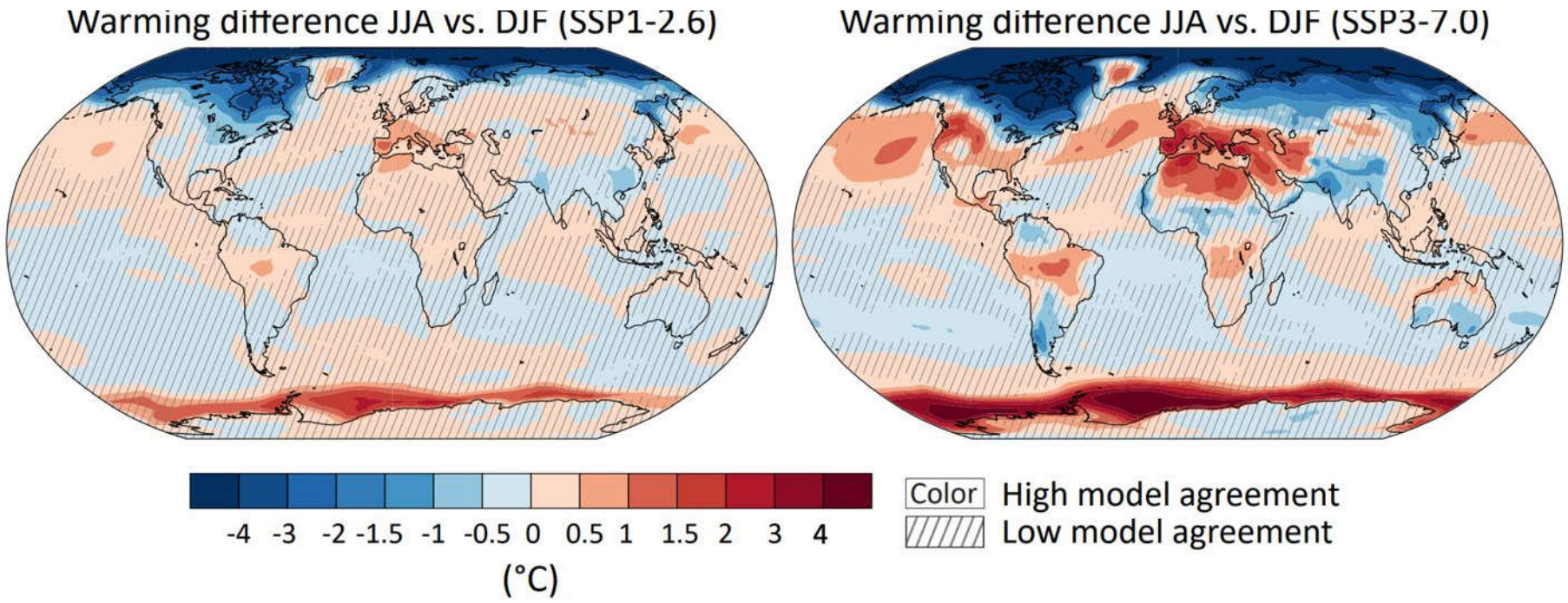

IPCC 2021, Chap. 4

Long-term change of annual and zonal mean atmospheric temperature

Figure 4.22: Long-term change of annual and zonal mean atmospheric temperature. Displayed are multi-model mean change in annual and zonal mean atmospheric temperature (°C) in 2081–2100 relative to 1995–2014 for (left) SSP1-2.6 and (right) SSP5-8.5. The number of models used is indicated in the top right of the maps. Diagonal lines indicate regions where less than 80% of the models agree on the sign of the change and no overlay where 80% or more of the models agree on the sign of the change. Further details on data sources and processing are available in the chapter data table (Table 4.SM.1).

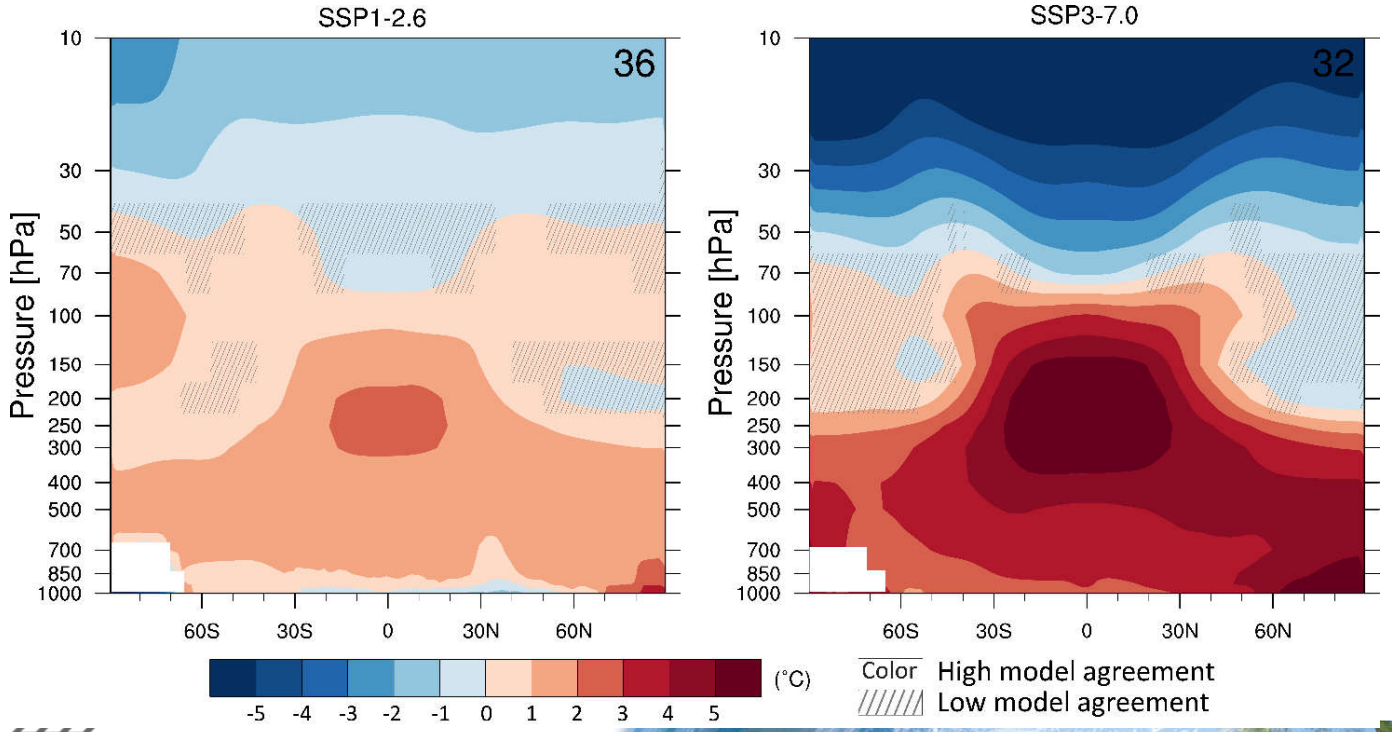

IPCC 2021, Chap. 4

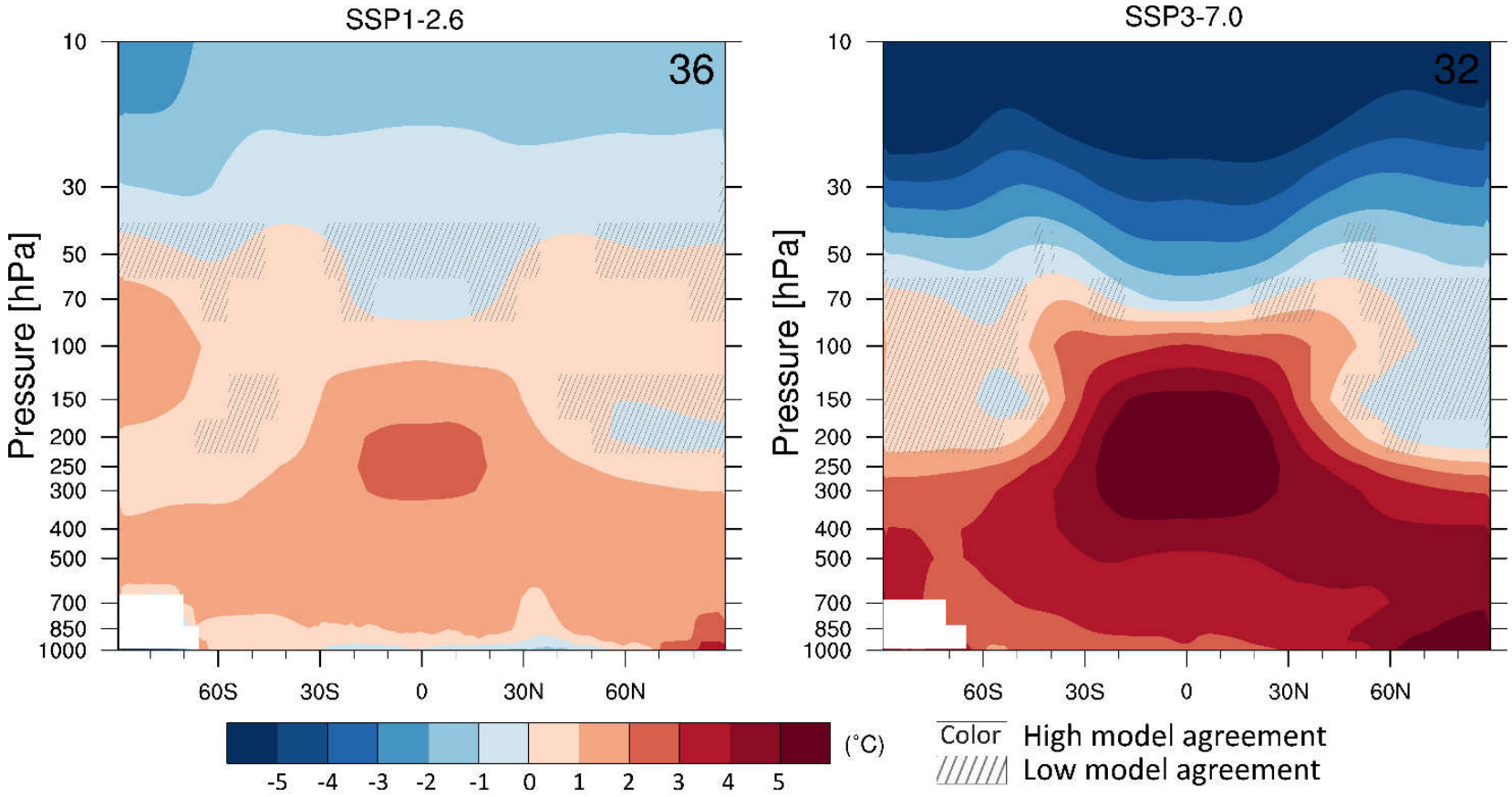

IPCC 2021, Chap. 4

Statements in the Executive Summary

Precipitation (1)

Annual global land precipitation will increase over the 21st century as GSAT increases (*high confidence*). The likely range of change in globally averaged annual land precipitation during 2081– 2100 relative to 1995–2014 is –0.2–4.7% in the low-emission scenario SSP1-1.9 and 0.9–12.9% in the high-emission scenario SSP5-8.5, based on all available CMIP6 models. The corresponding *likely* ranges are 0.0–6.6% in SSP1-2.6, 1.5–8.3% in SSP2-4.5, and 0.5–9.6% in SSP3-7.0. {4.3.1, 4.5.1, 4.6.1, 8.4.1}

IPCC 2021, Chap. 4

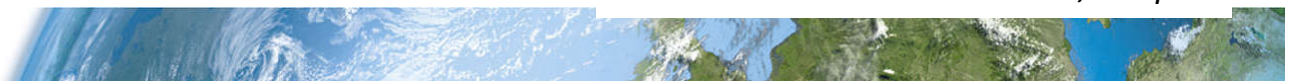

Selected indicators of global climate change from CMIP6 historical and scenario simulations

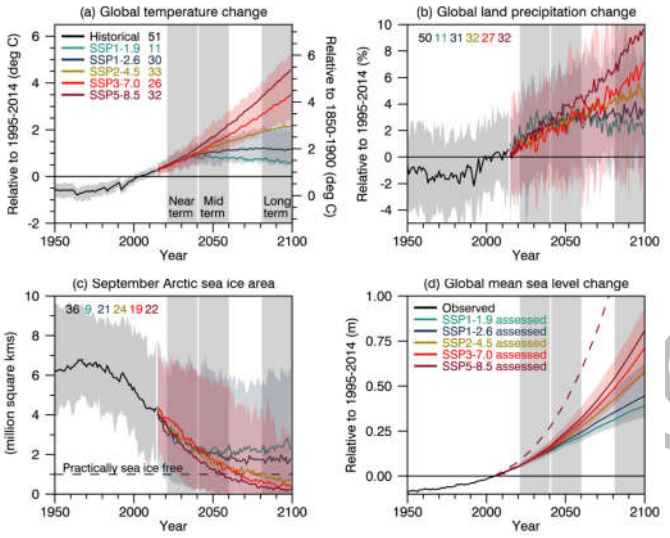

Figure 4.2: **Selected indicators of global climate change from CMIP6 historical and scenario simulations.** (a) Global surface air temperature changes relative to the 1995–2014 average (left axis) and relative to the 1850–1900 average (right axis; offset by 0.82°C, which is the multi-model mean and close to observed best estimate, Cross-Chapter Box 2.1, Table 1). (b) Global land precipitation changes relative to the 1995–2014 average. (c) September Arctic sea-ice area. (d) Global mean sea-level change (GMSL) relative to the 1995–2014 average. (a), (b) and (d) are annual averages, (c) are September averages. In (a)-(c), the curves show averages over the CMIP6 simulations, the shadings around the SSP1-2.6 and SSP3-7.0 curves show 5–95% ranges, and the numbers near the top show the number of model simulations used. Results are derived from concentration-driven simulations. In (d), the barystatic contribution to GMSL (i.e., the contribution from land-ice melt) has been added offline to the CMIP6 simulated contributions from thermal expansion (thermosteric). The shadings around the SSP1-2.6 and SSP3-7.0 curves show 5–95% ranges. The dashed curve is the *low confidence* and low likelihood outcome at the high end of SSP5-8.5 and reflects deep uncertainties arising from potential ice-sheet and ice-cliff instabilities. This curve at year 2100 indicates 1.7 m of GMSL rise relative to 1995–2014. More information on the calculation of GMSL are available in Chapter 9, and further regional details are provided in the Atlas. Further details on data sources and processing are available in the chapter data table (Table 4.SM.1).

IPCC 2021, Chap. 4

Global temperature and precipitation changea from CMIP6 historical and scenario simulations

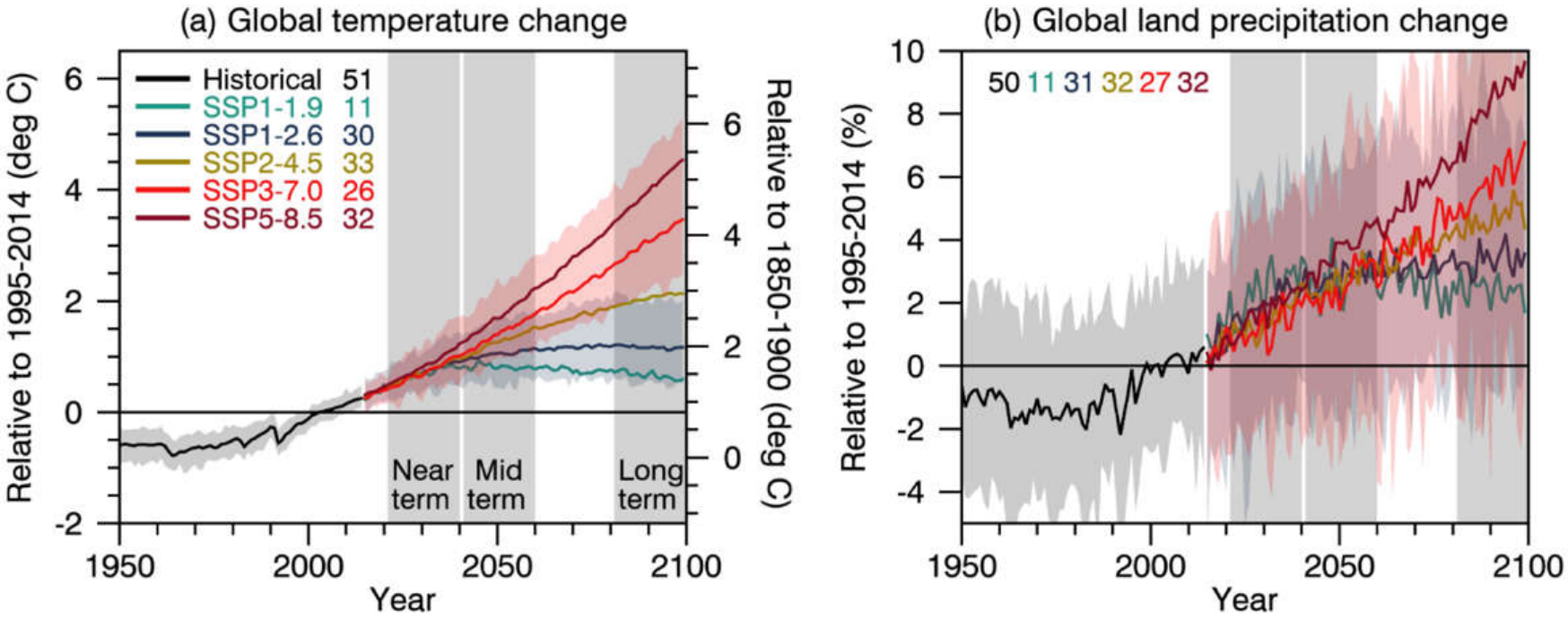

IPCC 2021, Chap. 4

Statements in the Executive Summary

Precipitation (1)

Annual global land precipitation will increase over the 21st century as GSAT increases (*high confidence*). The likely range of change in globally averaged annual land precipitation during 2081– 2100 relative to 1995–2014 is –0.2–4.7% in the low-emission scenario SSP1-1.9 and 0.9–12.9% in the high-emission scenario SSP5-8.5, based on all available CMIP6 models. The corresponding *likely* ranges are 0.0–6.6% in SSP1-2.6, 1.5–8.3% in SSP2-4.5, and 0.5–9.6% in SSP3-7.0. {4.3.1, 4.5.1, 4.6.1, 8.4.1}

Precipitation change will exhibit substantial regional differences and seasonal contrast as GSAT increases over the 21st century (*high confidence*). As warming increases, a larger land area will experience statistically significant increases or decreases in precipitation (*medium confidence*). Precipitation will *very likely* increase over high latitudes and the tropical oceans, and *likely* increase in large parts of the monsoon region, but *likely* decrease over large parts of the subtropics in response to greenhouse gas-induced warming. Interannual variability of precipitation over many land regions will increase with global warming (*medium confidence*). {4.5.1, 4.6.1, 8.4.1}

IPCC 2021, Chap. 4

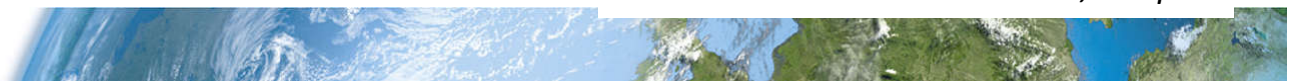

CMIP6 annual mean precipitation changes (%) from historical and scenario simulations

Figure 4.4: **CMIP6 annual mean precipitation changes (%) from historical and scenario simulations**. (a) Northern Hemisphere extratropics (30°N–90°N). (b) North Atlantic subtropics (5°N–30°N, 80°W–0°). Changes are relative to 1995–2014 averages. Displayed are multi-model averages and, in parentheses, 5–95% ranges. The numbers inside each panel are the number of model simulations. Results are derived from concentration-driven simulations. Further details on data sources and processing are available in the chapter data table (Table 4.SM.1).

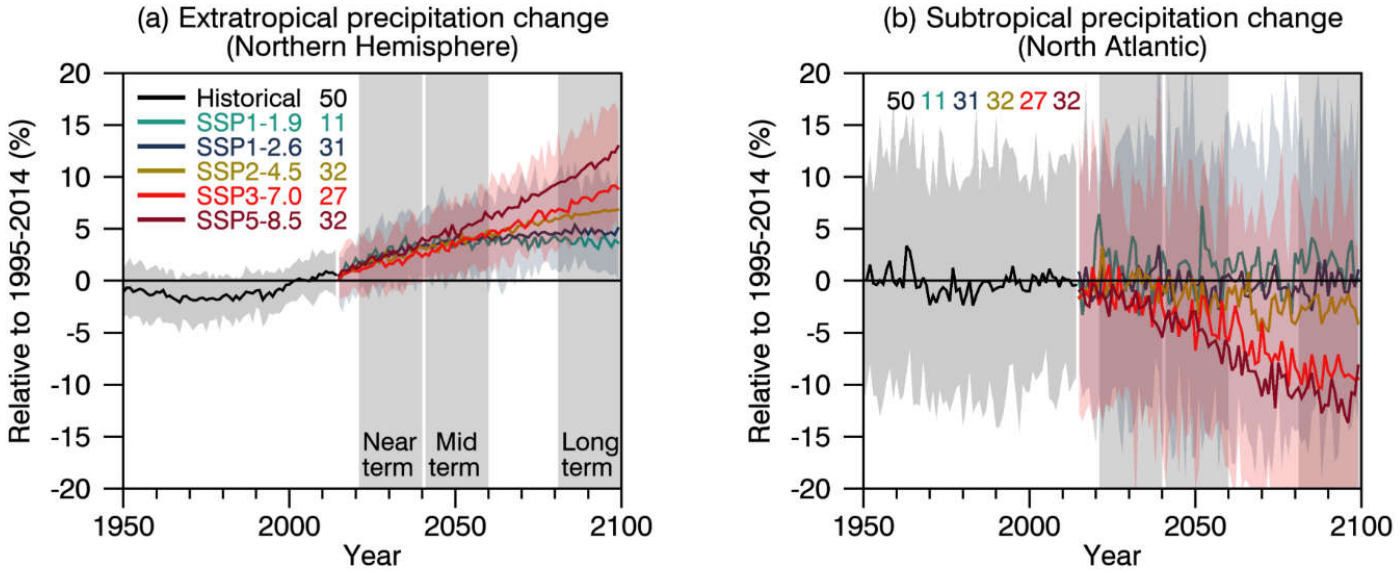

IPCC 2021, Chap. 4

CMIP6 annual mean precipitation changes (%) from historical and scenario simulations

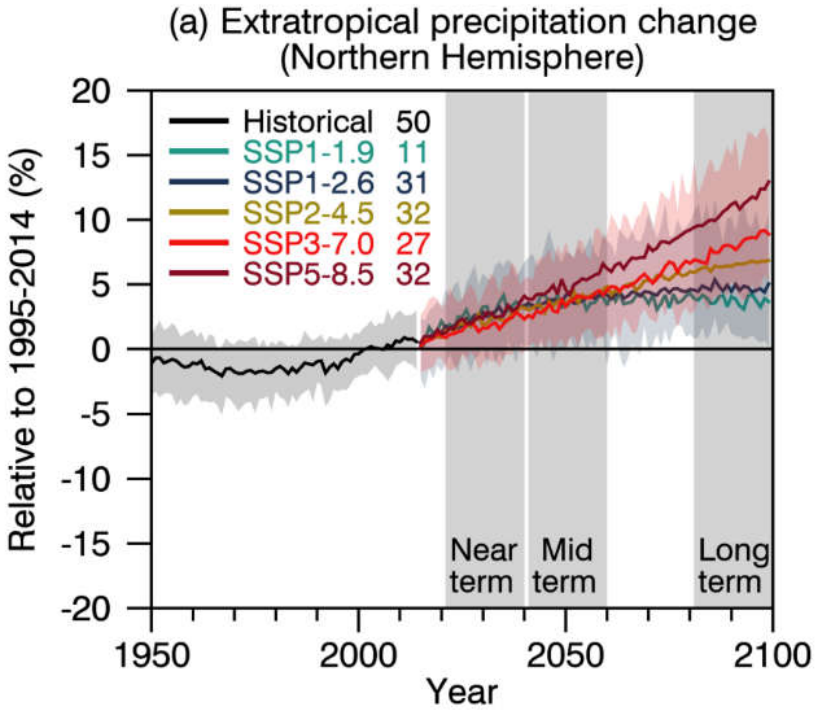

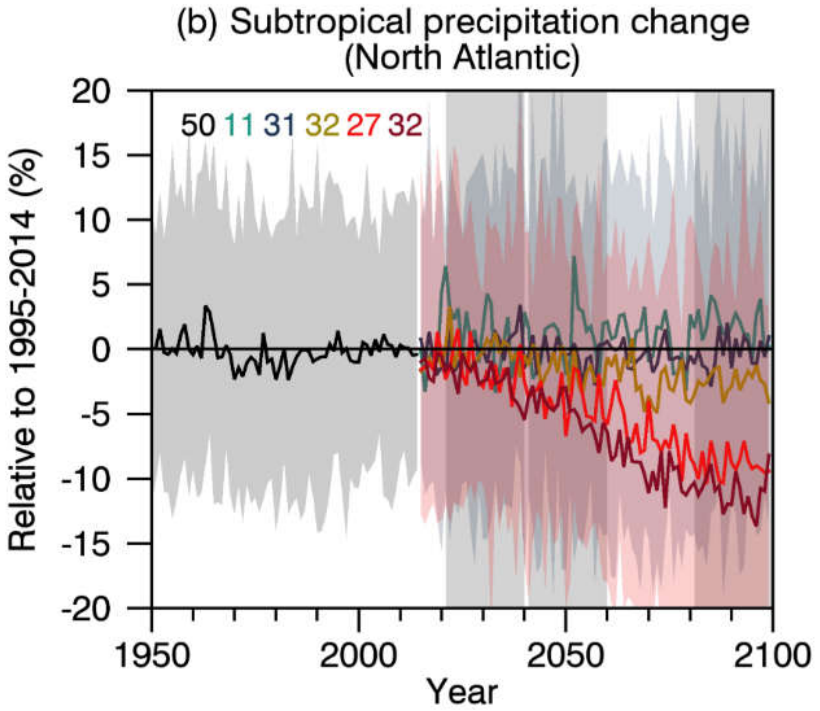

IPCC 2021, Chap. 4

Projected spatial patterns of change in annual average precipitation (expressed as a percentage change) at different levels of global warming

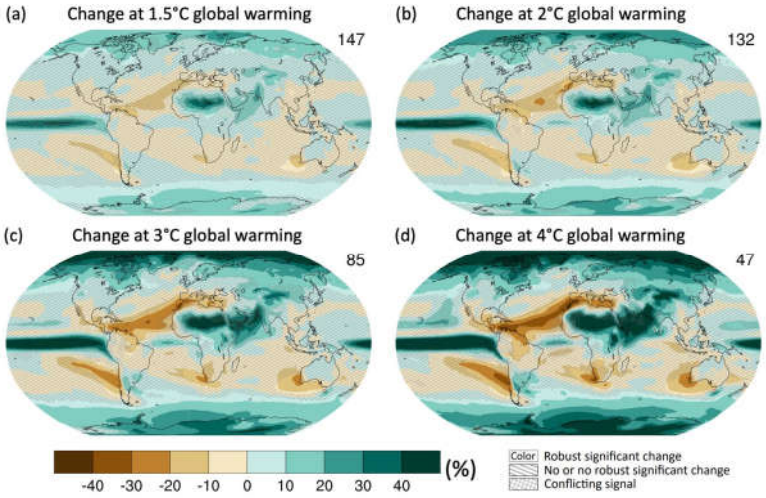

Figure 4.32: Projected spatial patterns of change in annual average precipitation (expressed as a percentage change) at different levels of global warming. Displayed are (a–d) spatial patterns of change in annual precipitation at 1.5°C, 2°C, 3°C, and 4°C of global warming reletive to the period 1850–1900. No map overlay indicates regions where the change is robust and *likely* emerges from internal variability, that is, where at least 66% of the models show a change greater than the internal-variability threshold (see Section 4.2.6) and at least 80% of the models agree on the sign of change. Diagonal lines indicate regions with no change or no robust significant change, where fewer than 66% of the models show change greater than the internal-variability threshold. Crossed lines indicate areas of conflicting signals where at least 66% of the models show change greater than the internal-variability threshold but fewer than 80% of all models agree on the sign of change. Values were assessed from a 20-year period at a given warming level, based on model simulations under the Tier-1 SSPs of CMIP6. Further details on data sources and processing are available in the chapter data table (Table 4.SM.1).

IPCC 2021, Chap. 4

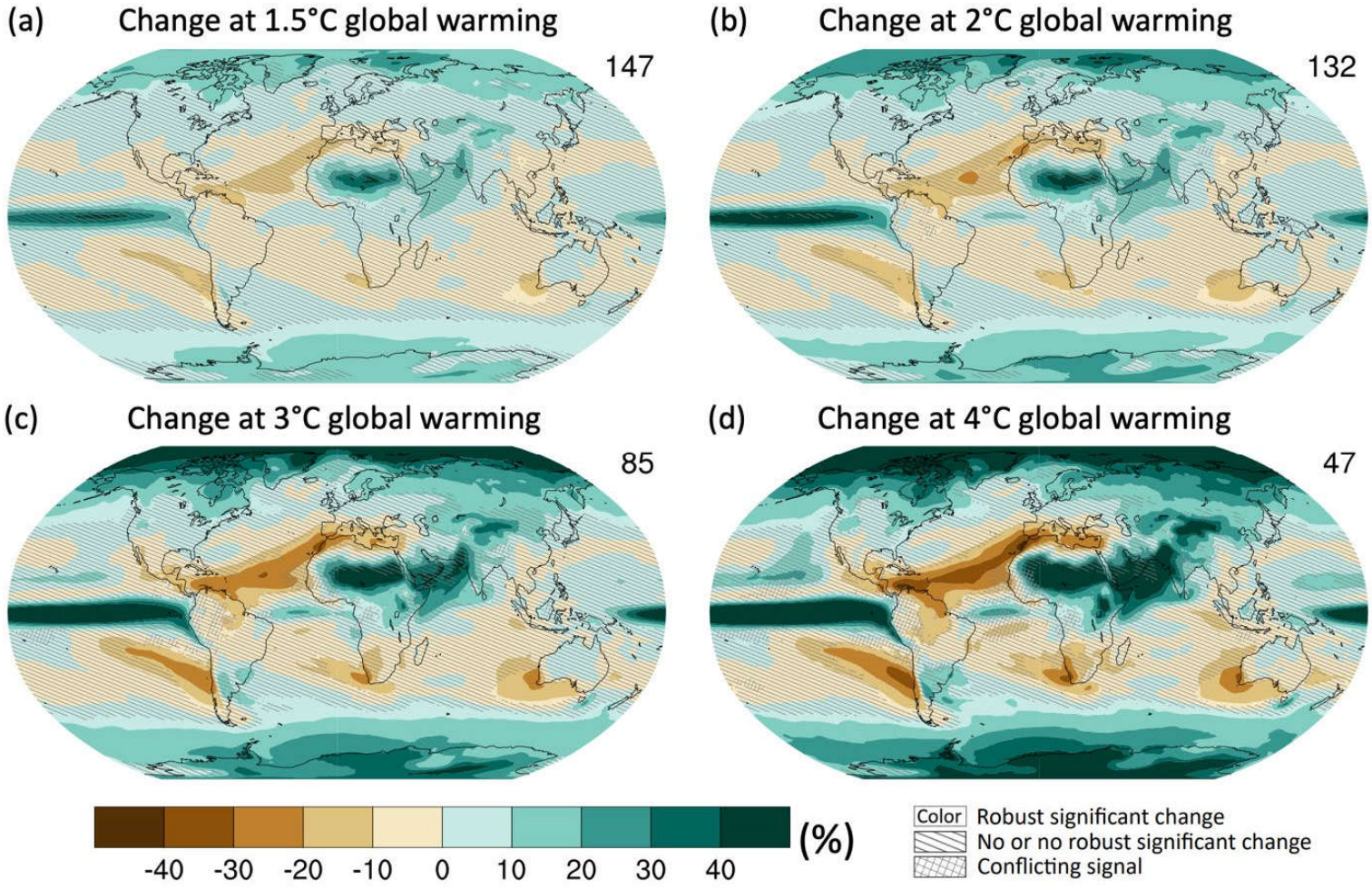

IPCC 2021, Chap. 4

Long-term changes in seasonal mean relative humidity

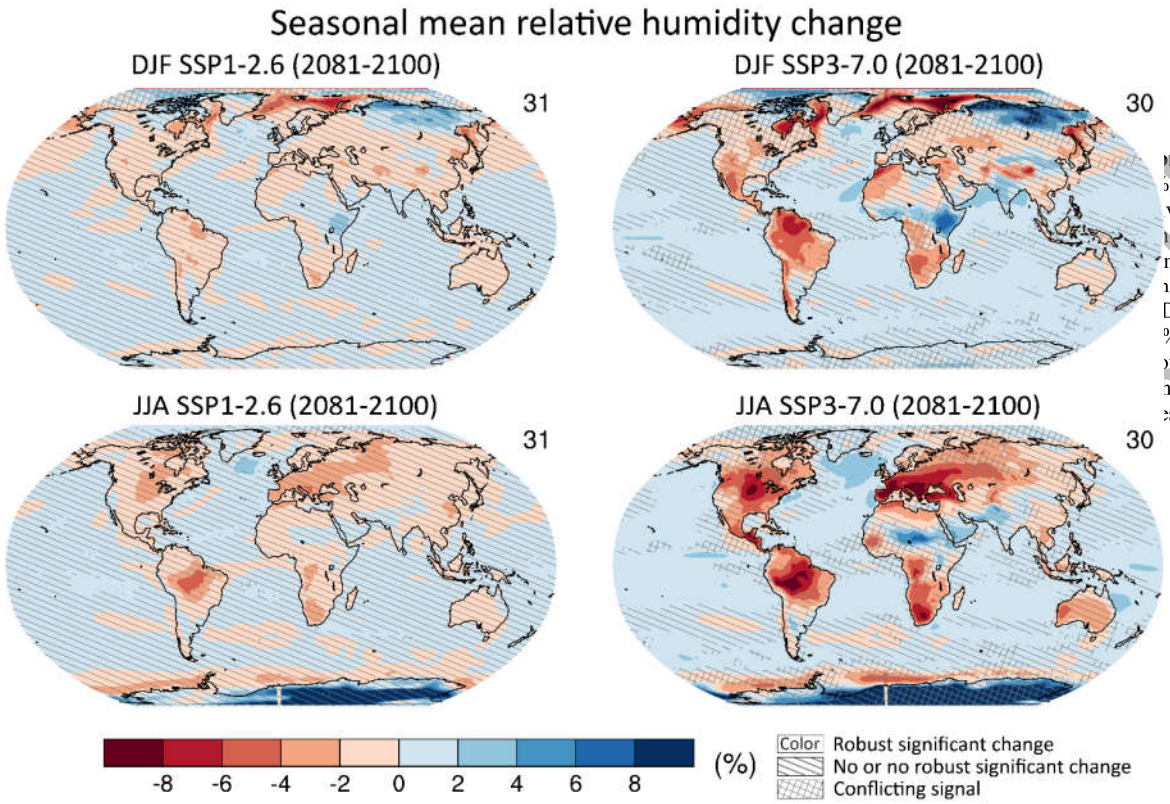

…nal mean relative humidity. Displayed are projected spatial patterns of …) in seasonal (top) DJF and (bottom) JJA mean near-surface relative …ve to 1995–2014, for (left) SSP1-2.6 and (right) SSP3-7.0. The number of …e top right of the maps. No overlay indicates regions where the change is …m internal variability, that is, where at least 66% of the models show a …al-variability threshold (see Section 4.2.6) and at least 80% of the models … Diagonal lines indicate regions with no change or no robust significant …% of the models show change greater than the internal-variability threshold. …f conflicting signals where at least 66% of the models show change greater …reshold but fewer than 80% of all models agree on the sign of change. …s and processing are available in the chapter data table (Table 4.SM.1).

IPCC 2021, Chap. 4

Seasonal mean relative humidity change

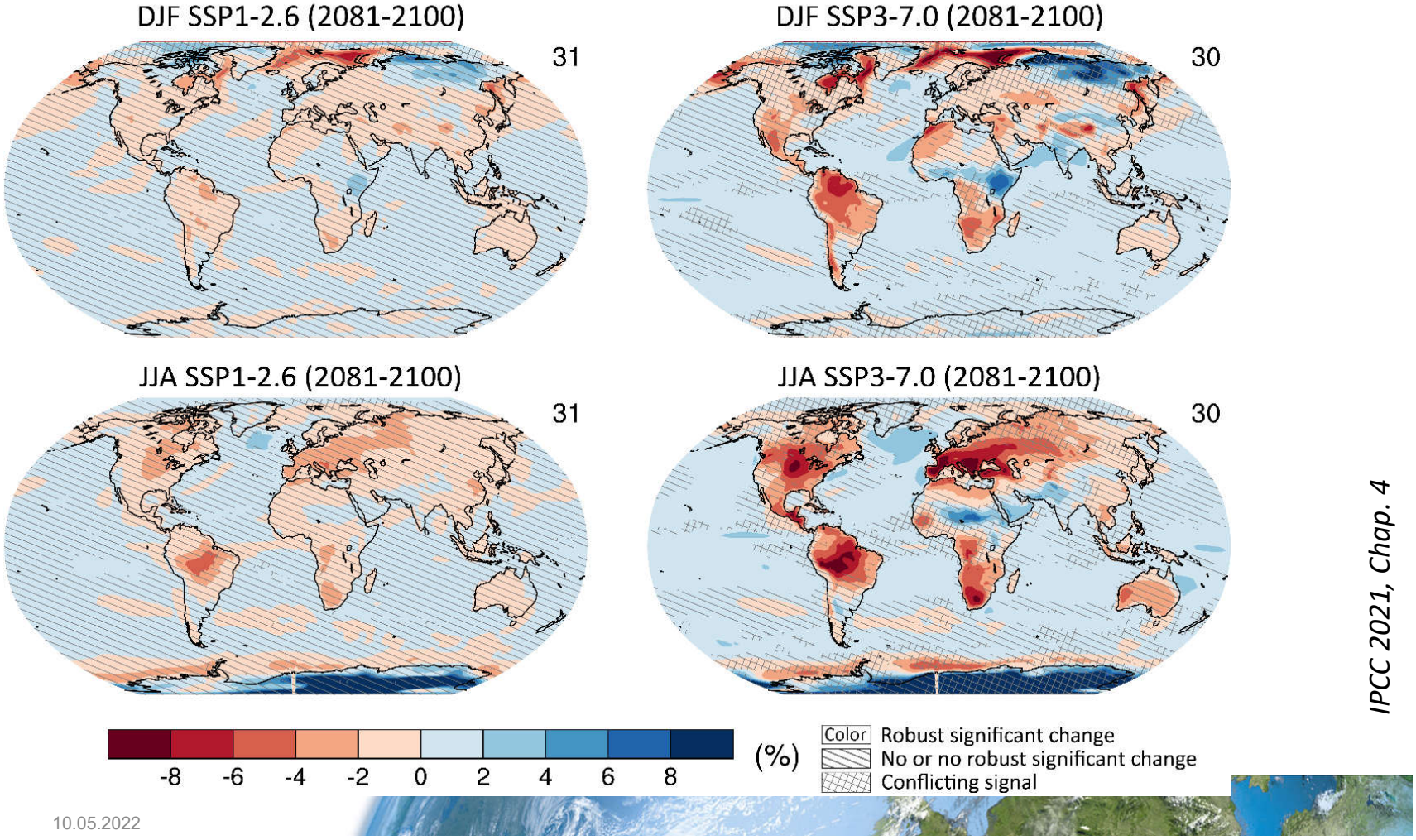

IPCC 2021, Chap. 4

Long-term change of seasonal mean precipitation

Figure 4.24: Long-term change of seasonal mean precipitation. Displayed are projected spatial patterns of multi-model mean change (%) in (top) DJF and (bottom) JJA mean precipitation in 2081–2100 relative to 1995–2014, for (left) SSP1-2.6 and (right) SSP3-7.0. The number of models used is indicated in the top right of the maps. No map overlay indicates regions where the change is robust and *likely* emerges from internal variability, that is, where at least 66% of the models show a change greater than the internal-variability threshold (see Section 4.2.6) and at least 80% of the models agree on the sign of change. Diagonal lines indicate regions with no change or no robust significant change, where fewer than 66% of the models show change greater than the internal-variability threshold. Crossed lines indicate areas of conflicting signals where at least 66% of the models show change greater than the internal-variability threshold but fewer than 80% of all models agree on the sign of change. Further details on data sources and processing are available in the chapter data table (Table 4.SM.1).

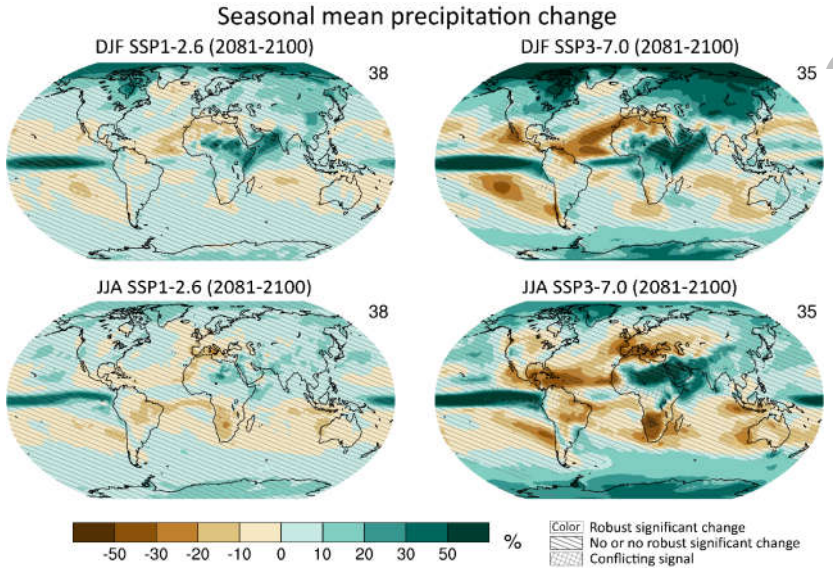

IPCC 2021, Chap. 4

Seasonal mean precipitation change

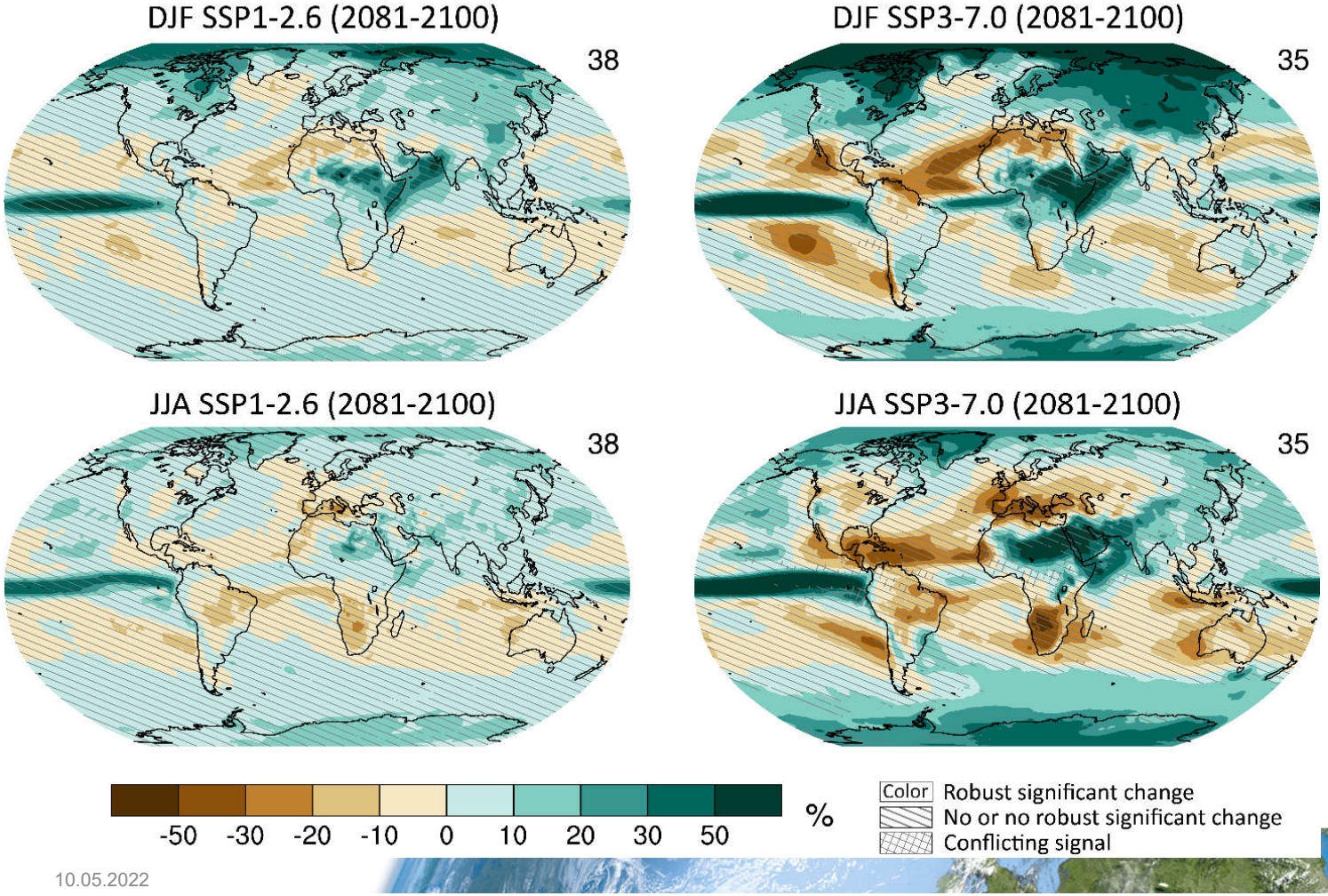

IPCC 2021, Chap. 4

Regional changes in temperature (left) and precipitation (right) are proportional to the level of global warming

FAQ 4.3, Figure 1: Regional changes in temperature (left) and precipitation (right) are proportional to the level of global warming, irrespective of the scenario through which the level of global warming is reached. Surface warming and precipitation change are shown relative to the 1850–1900 climate, and for time periods over which the globally averaged surface warming is 1.5°C (top) and 3°C (bottom), respectively. Changes presented here are based on thirty-one CMIP6 models using the high-emission scenario SSP3-7.0.

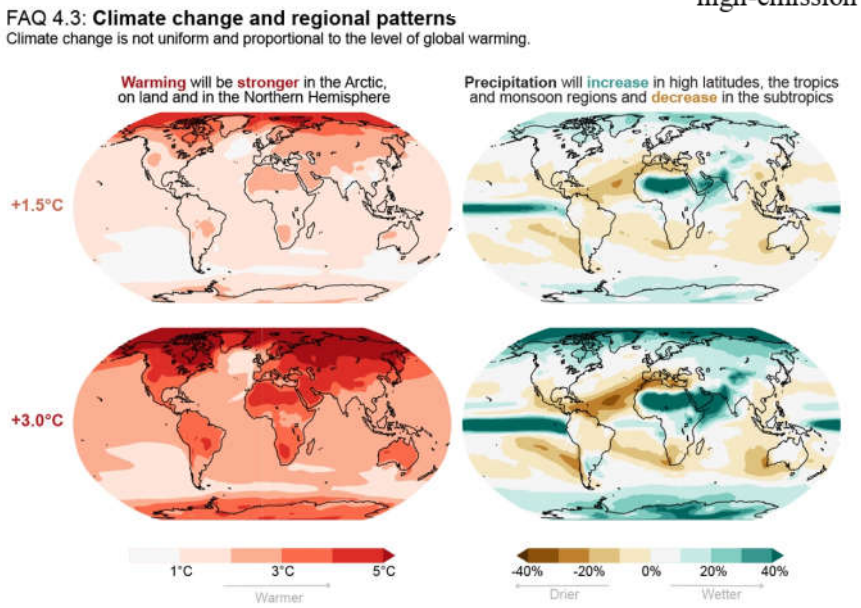

IPCC 2021, Chap. 4

FAQ 4.3: **Climate change and regional patterns**

Climate change is not uniform and proportional to the level of global warming.

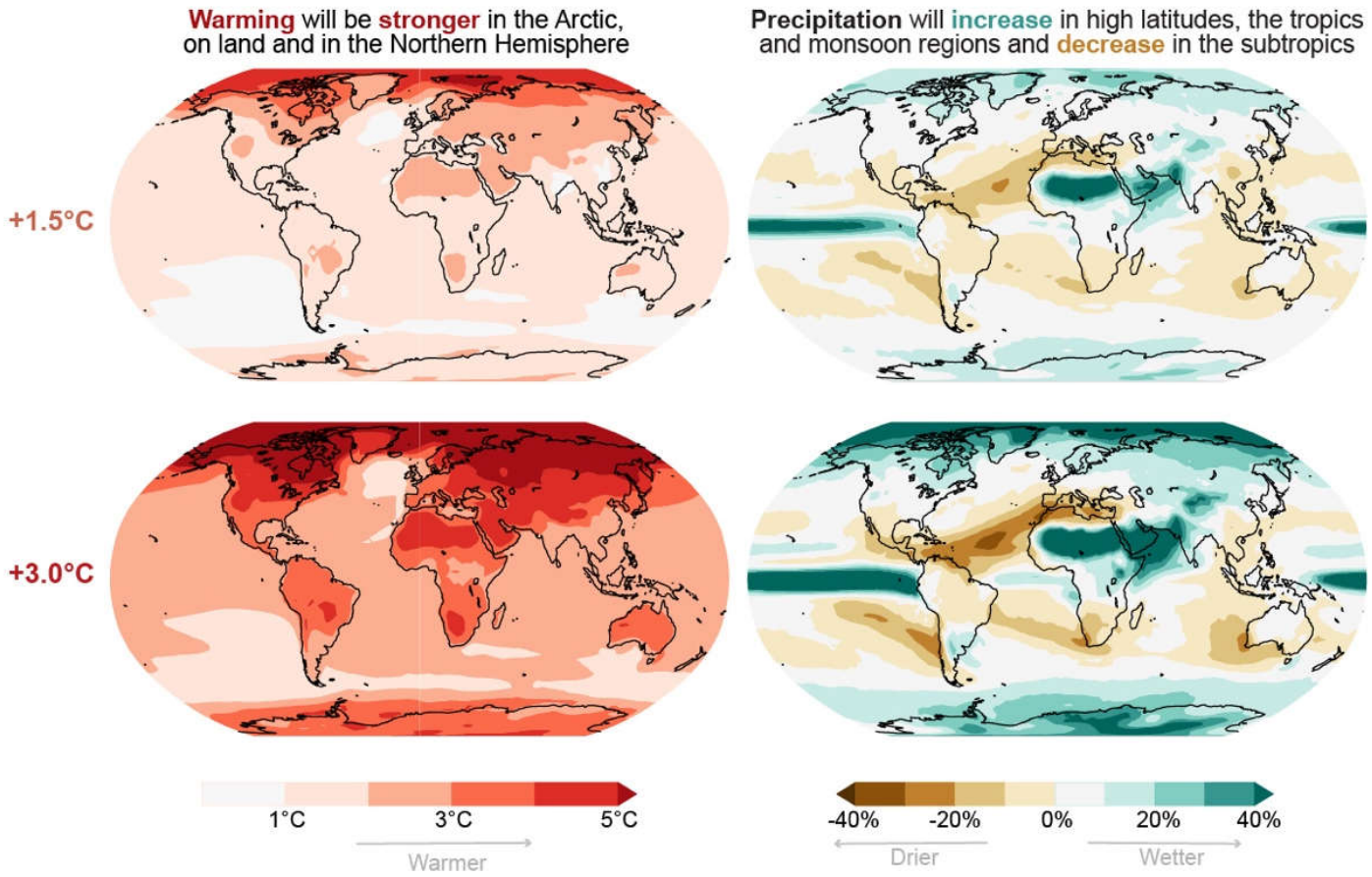

IPCC 2021, Chap. 4

Statements in the Executive Summary

Precipitation (2)

Near-term projected changes in precipitation are uncertain, mainly because of natural internal variability, model uncertainty, and uncertainty in natural and anthropogenic aerosol forcing (*medium confidence*). In the near term, no discernible differences in precipitation changes are projected between different SSPs (*high confidence*). The anthropogenic aerosol forcing decreases in most scenarios, contributing to increases in GSAT (*medium confidence*) and global-mean land precipitation (*low confidence*). {4.3.1, 4.4.1, 4.4.4, 8.5}

Near-term change of seasonal mean precipitation

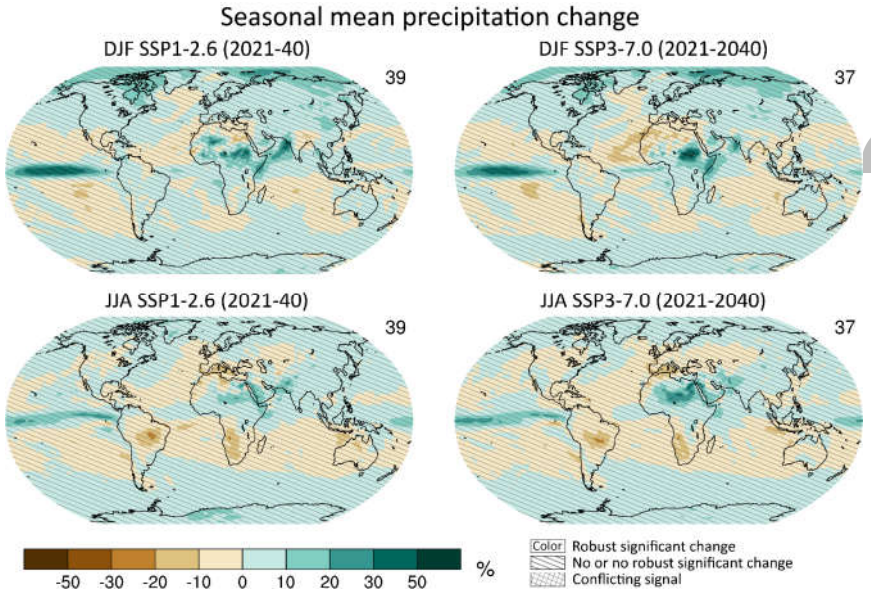

Figure 4.13: Near-term change of seasonal mean precipitation. Displayed are projected spatial patterns of CMIP6 multi-model mean change (%) in (top) DJF and (bottom) JJA precipitation from SSP1-2.6 and SSP3-7.0 in 2021–2040 relative to 1995–2014. The number of models used is indicated in the top right of the maps. No overlay indicates regions where the change is robust and *likely* emerges from internal variability, that is, where at least 66% of the models show a change greater than the internal-variability threshold (see Section 4.2.6) and at least 80% of the models agree on the sign of change. Diagonal lines indicate regions with no change or no robust significant change, where fewer than 66% of the models show change greater than the internal-variability threshold. Crossed lines indicate areas of conflicting signals where at least 66% of the models show change greater than the internal-variability threshold but fewer than 80% of all models agree on the sign of change. Further details on data sources and processing are available in the chapter data table (Table 4.SM.1).

IPCC 2021, Chap. 4

Seasonal mean precipitation change

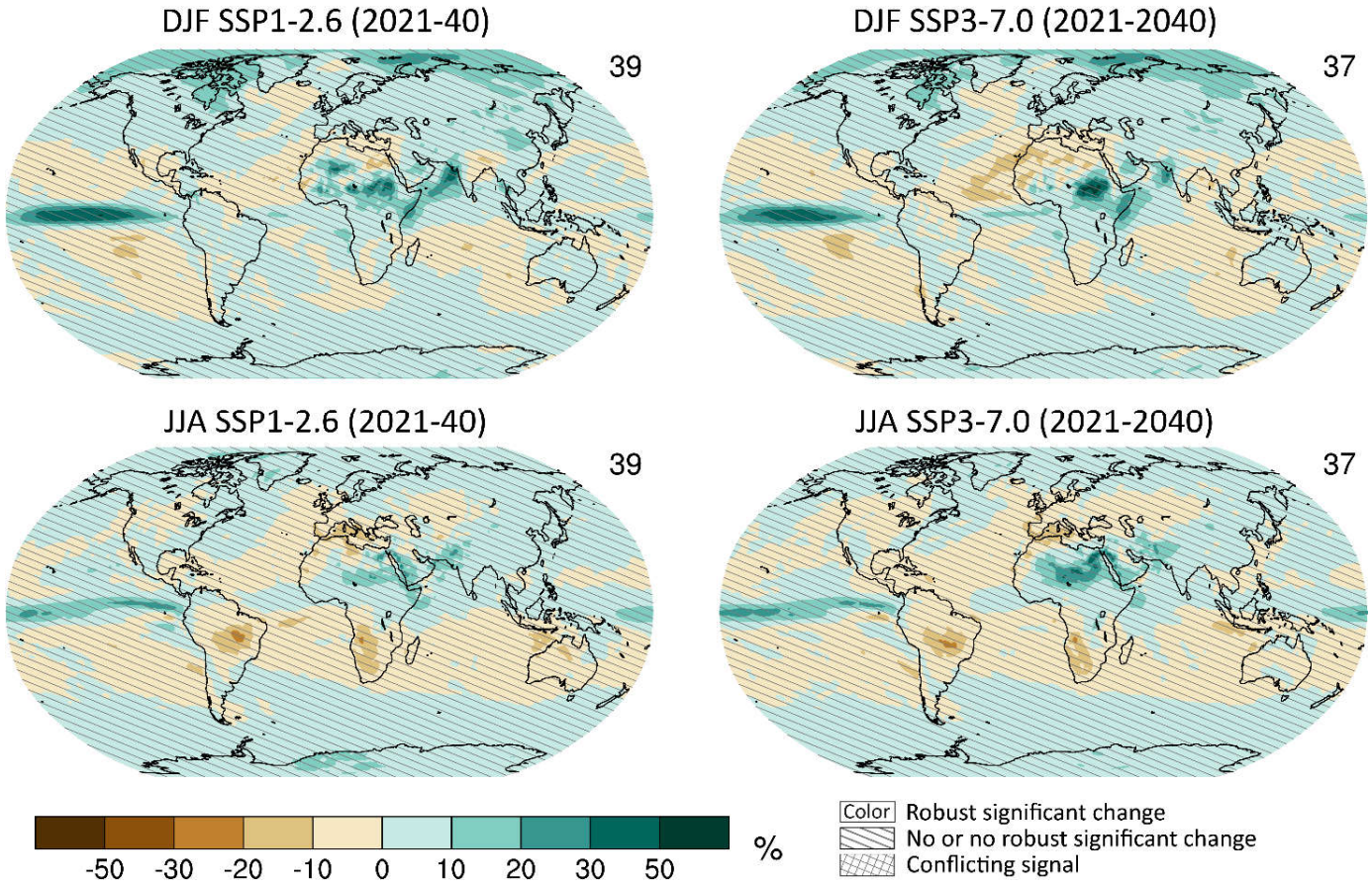

IPCC 2021, Chap. 4

Statements in the Executive Summary

Precipitation (3)

In response to greenhouse gas-induced warming, it is *likely* that global land monsoon precipitation will increase, particularly in the Northern Hemisphere, although Northern Hemisphere monsoon circulation will *likely* weaken. In the long term (2081–2100), monsoon rainfall change will feature a north–south asymmetry characterized by a greater increase in the Northern Hemisphere than in the Southern Hemisphere and an east–west asymmetry characterized by an increase in Asian-African monsoon regions and a decrease in the North American monsoon region (*medium confidence*). Near-term changes in global monsoon precipitation and circulation are uncertain due to model uncertainty and internal variability such as Atlantic Multi-decadal Variability and Pacific Decadal Variability (*medium confidence*). {4.4.1, 4.5.1, 8.4.1, 10.6.3}

Time series of global land monsoon precipitation and Northern Hemisphere summer monsoon (NHSM) circulation index anomalies.

Figure 4.14: Time series of global land monsoon precipitation and Northern Hemisphere summer monsoon (NHSM) circulation index anomalies. (a) Global land monsoon precipitation index anomalies (Unit: %) defined as the area-weighted mean precipitation rate in the global land monsoon domain defined by Wang et al. (2013) for the CMIP6 historical simulation for 1950–2014 and five SSPs 2015–2100. (b) Anomalies in NHSM circulation index (Unit: m s^{-1}), defined as the vertical shear of zonal winds between 850 and 200 hPa averaged in a zone stretching from Mexico eastward to the Philippines (0°–20°N, 120°W–120°E) (Wang et al., 2013) in the CMIP6 historical simulation and five SSPs. One realization is averaged from each model. Anomalies are shown relative to the present-day (1995–2014) mean. The curves show averages over the simulations, the shadings around the SSP1-2.6 and SSP5-8.5 curves show 5–95% ranges, and the numbers near the top show the number of model simulations used. Further details on data sources and processing are available in the chapter data table (Table 4.SM.1).

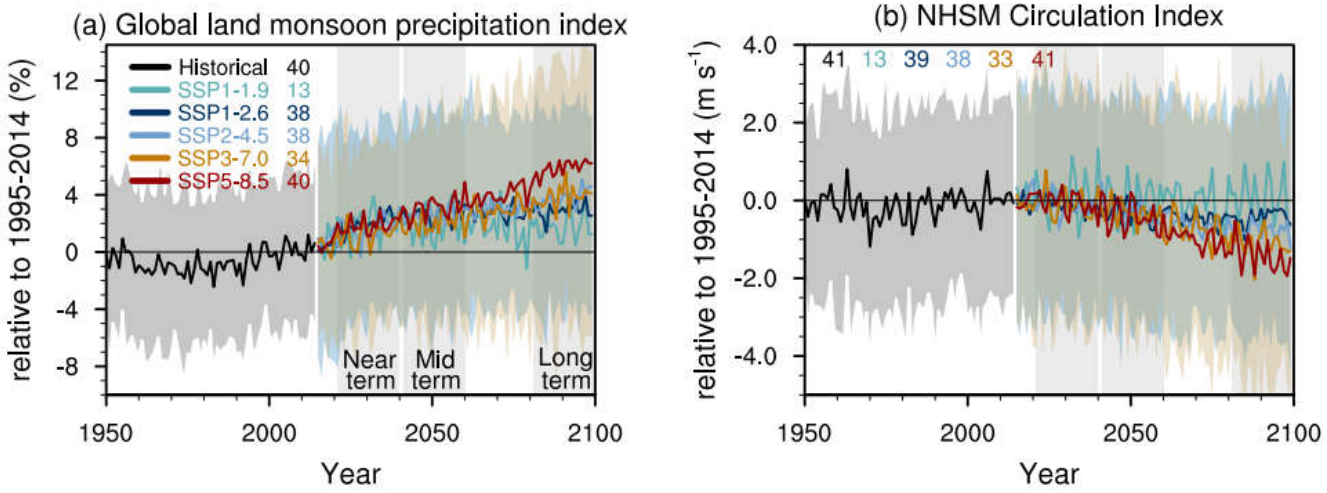

IPCC 2021, Chap. 4

Time series of global land monsoon precipitation and Northern Hemisphere summer monsoon (NHSM) circulation index anomalies.

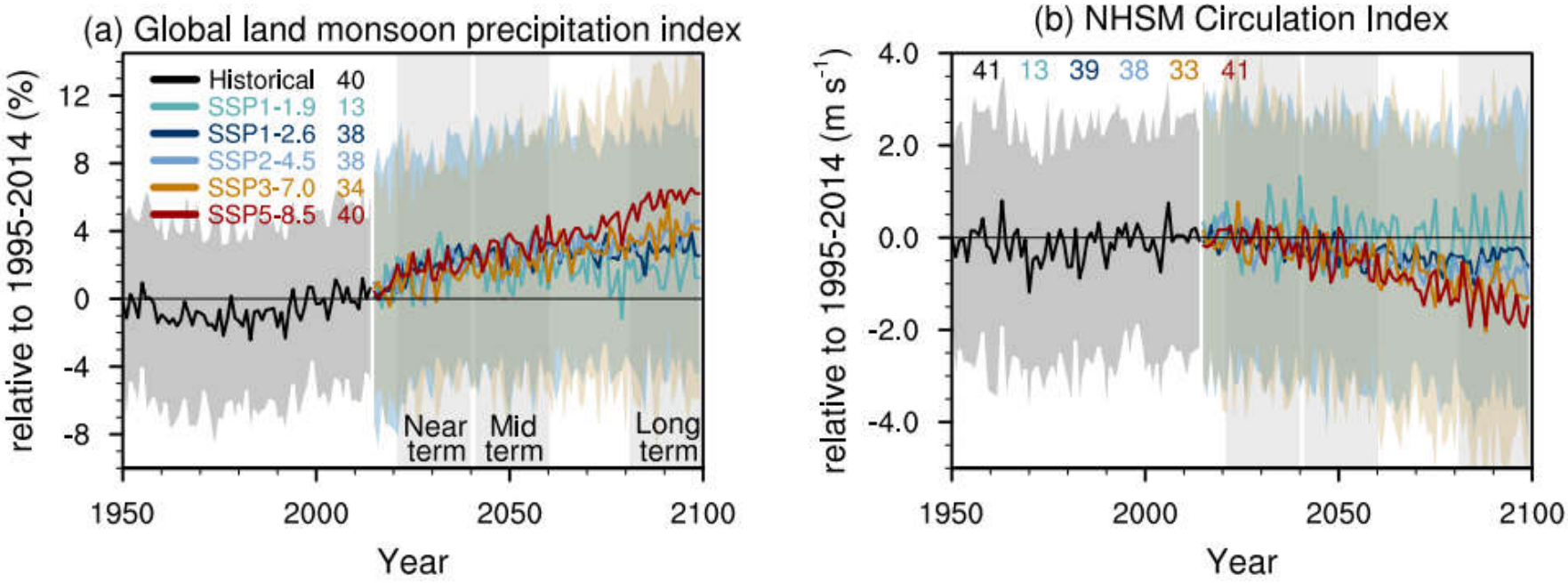

IPCC 2021, Chap. 4

Statements in the Executive Summary

Precipitation (4)

It is likely that at least one large volcanic eruption will occur during the 21st century. Such an eruption would reduce GSAT for several years, decrease global-mean land precipitation, alter monsoon circulation, modify extreme precipitation, and change the profile of many regional climatic impact-drivers. A low-likelihood, high-impact outcome would be several large eruptions that would greatly alter the 21st century climate trajectory compared to SSP-based Earth system model projections. {Cross-Chapter Box 4.1}

Modes of variability (1)

The **Southern Annular Mode (SAM)** is a climate driver that can influence rainfall and temperature in Australia. The SAM refers to the (non-seasonal) north-south movement of the strong westerly winds that blow almost continuously in the mid- to high-latitudes of the southern hemisphere. The station-based index of the SAM is based on the zonal pressure difference between the latitudes of 40S and 65S.

The **Arctic oscillation (AO)** or **Northern Annular Mode/Northern Hemisphere Annular Mode (NAM)** is a weather phenomenon at the Arctic pole north of 20 degrees latitude. It is an important mode of climate variability for the Northern Hemisphere. The southern hemisphere analogue is called the Antarctic oscillation or Southern Annular Mode (SAM). The index varies over time with no particular periodicity, and is characterized by non-seasonal sea-level pressure anomalies of one sign in the Arctic, balanced by anomalies of opposite sign centered at about 37–45°N

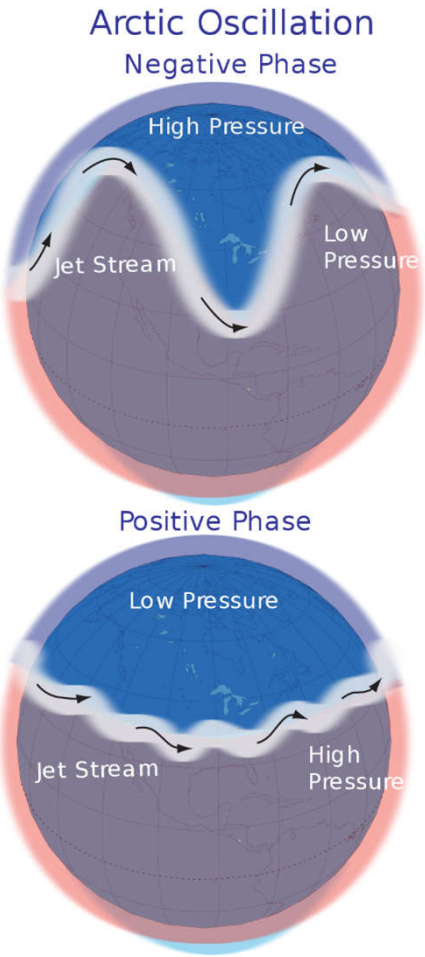

Statements in the Executive Summary

Large-scale Circulation and Modes of Variability (1)

In the near term, the forced change in Southern Annular Mode in austral summer is *likely* to be weaker than observed during the late 20th century under all five SSPs assessed. This is because of the opposing influence in the near- to mid-term from stratospheric ozone recovery and increases in other greenhouse gases on the Southern Hemisphere summertime mid-latitude circulation (*high confidence*). In the near term, forced changes in the Southern Annular Mode in austral summer are therefore *likely* to be smaller than changes due to natural internal variability. {4.3.3, 4.4.3}

IPCC 2021, Chap. 4

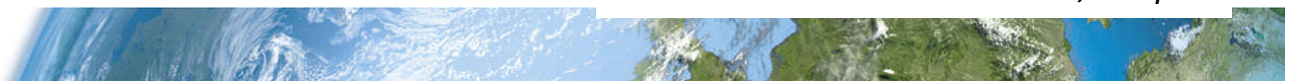

CMIP6 Annular Mode index change (hPa) from 1995–2014 to 2021–2040

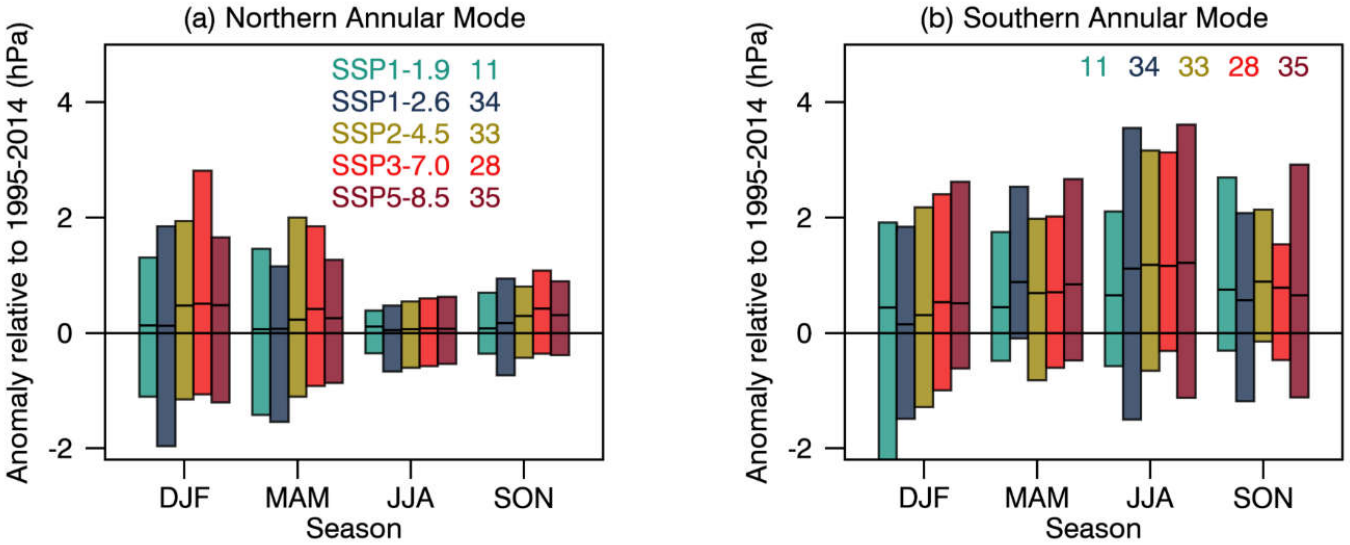

Figure 4.17: CMIP6 Annular Mode index change (hPa) from 1995–2014 to 2021–2040. (a) NAM and (b) SAM. The NAM is defined as the difference in zonal mean sea-level pressure (SLP) at 35°N and 65°N (Li and Wang, 2003) and the SAM as the difference in zonal mean SLP at 40°S and 65°S (Gong and Wang, 1999). The shadings are the 5–95% ranges across the simulations. The numbers near the top of each panel are the numbers of model simulations in each SSP ensemble. Further details on data sources and processing are available in the chapter data table (Table 4.SM.1).

IPCC 2021, Chap. 4

CMIP6 Annular Mode index change (hPa) from 1995–2014 to 2021–2040

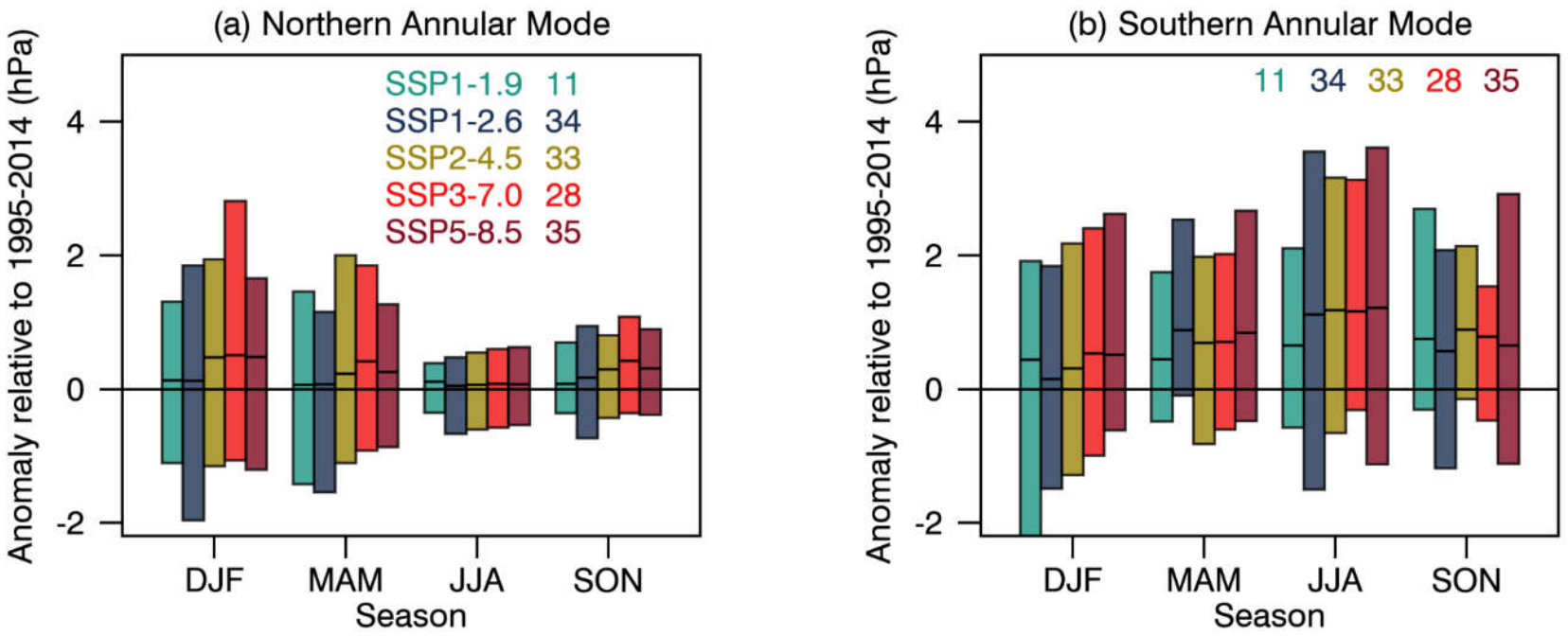

IPCC 2021, Chap. 4

Statements in the Executive Summary

Large-scale Circulation and Modes of Variability (1)

In the near term, the forced change in Southern Annular Mode in austral summer is *likely* to be weaker than observed during the late 20th century under all five SSPs assessed. This is because of the opposing influence in the near- to mid-term from stratospheric ozone recovery and increases in other greenhouse gases on the Southern Hemisphere summertime mid-latitude circulation (*high confidence*). In the near term, forced changes in the Southern Annular Mode in austral summer are therefore *likely* to be smaller than changes due to natural internal variability. {4.3.3, 4.4.3}

In the long term, the Southern Hemisphere mid-latitude jet is *likely* to shift poleward and strengthen under SSP5-8.5 relative to 1995–2014. This is *likely* to be accompanied by an increase in the Southern Annular Mode index in all seasons relative to 1995–2014. For SSP1-2.6, CMIP6 models project no robust change in the Southern Annular Mode index in the long term. It is *likely* that wind speeds associated with extratropical cyclones will strengthen in the Southern Hemisphere storm track for SSP5-8.5. {4.5.1, 4.5.3}

IPCC 2021, Chap. 4

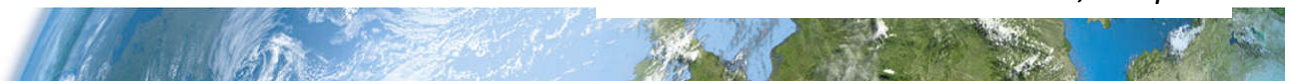

CMIP6 Annular Mode index change from 1995–2014 to 2081–2100

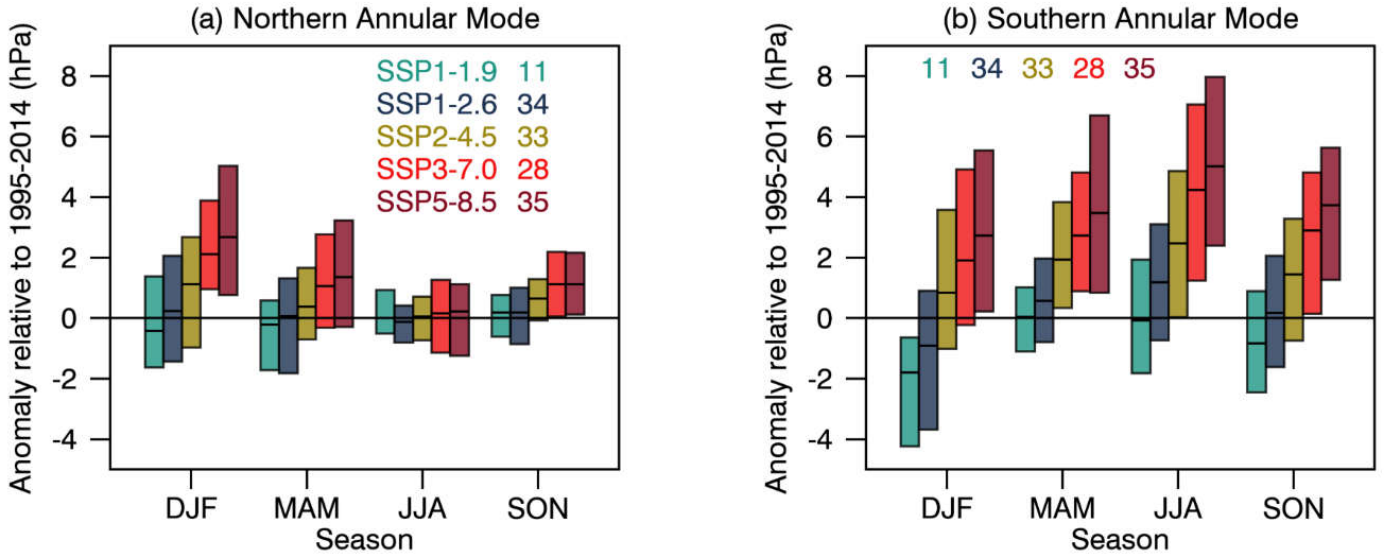

Figure 4.30: CMIP6 Annular Mode index change from 1995–2014 to 2081–2100: (a) NAM and (b) SAM. The NAM is defined as the difference in zonal mean SLP at 35°N and 65°N (Li and Wang, 2003) and the SAM as the difference in zonal mean SLP at 40°S and 65°S (Gong and Wang, 1999). The shadings are the 5–95% ranges across the simulations. The numbers near the top are the numbers of model simulations in each SSP ensemble. Further details on data sources and processing are available in the chapter data table (Table 4.SM.1).

IPCC 2021, Chap. 4

CMIP6 Annular Mode index change from 1995–2014 to 2081–2100

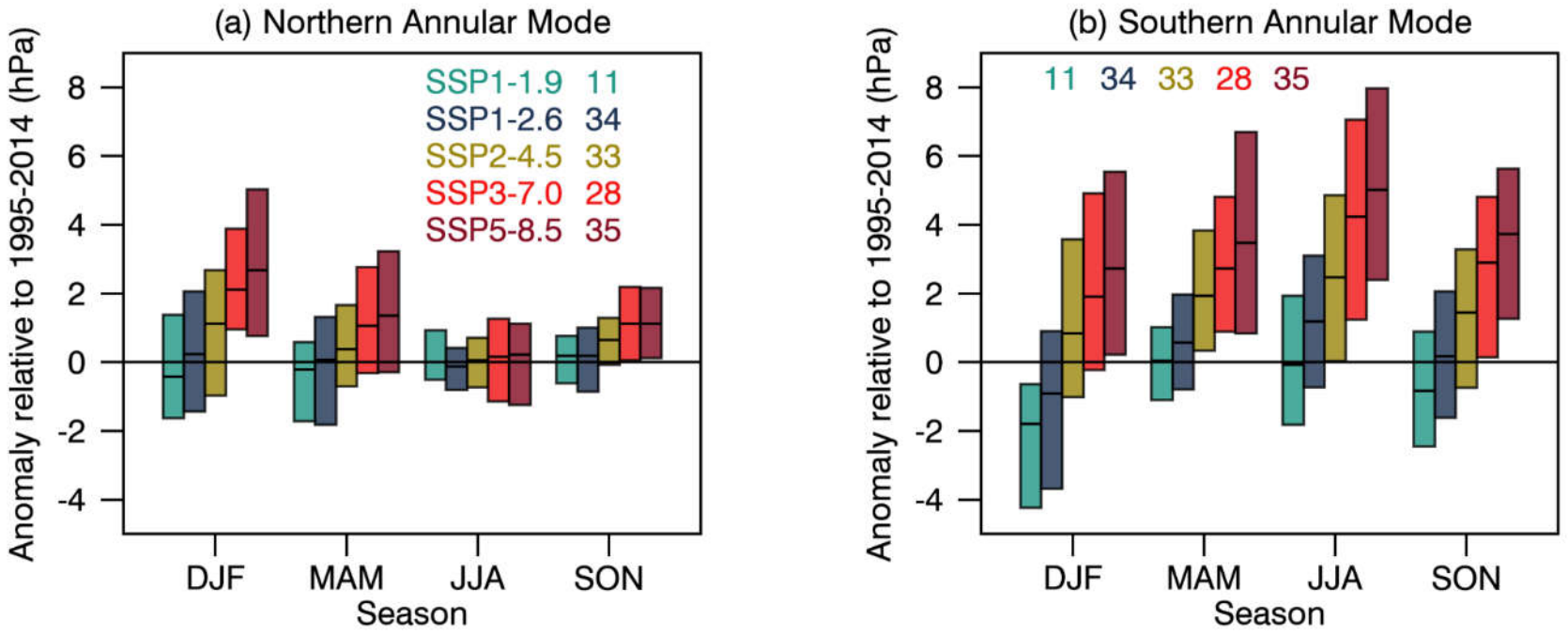

IPCC 2021, Chap. 4

Statements in the Executive Summary

Large-scale Circulation and Modes of Variability (2)

The CMIP6 multi-model ensemble projects a long-term increase in the boreal wintertime Northern Annular Mode index under the high-emission scenarios of SSP3-7.0 and SSP5-8.5, but regional changes may deviate from a simple shift in the mid-latitude circulation. Substantial uncertainty and thus *low confidence* remain in projecting regional changes in Northern Hemisphere jet streams and storm tracks, especially for the North Atlantic basin in winter; this is due to large natural internal variability, the competing effects of projected upper- and lower-tropospheric temperature gradient changes, and new evidence of weaknesses in simulating past variations in North Atlantic atmospheric circulation on seasonal-to-decadal timescales. One exception is the expected decrease in frequency of atmospheric blocking events over Greenland and the North Pacific in boreal winter in SSP3-7.0 and SSP5-8.5 scenarios (*medium confidence*). {4.5.1}

IPCC 2021, Chap. 4

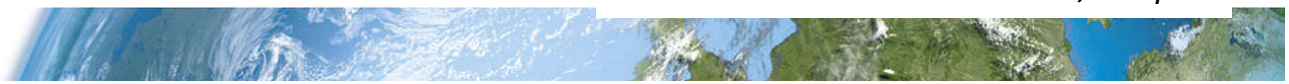

Long-term change of zonal mean zonal wind

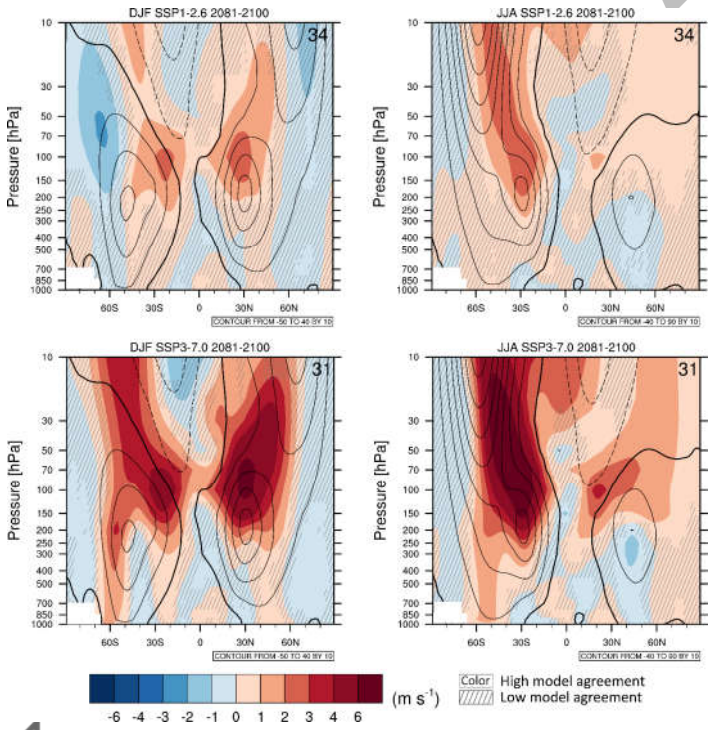

Figure 4.26: Long-term change of zonal mean zonal wind. Dispayed are multi-model mean change in (left) boreal winter (DJF) and (right) austral winter (JJA) zonal mean zonal wind (m s^{-1}) in 2081–2100 for (top) SSP1-2.6 and (right) SSP3-7.0 relative to 1995–2014. The 1995–2014 climatology is shown in contours with spacing 10 m s^{-1}. Diagonal lines indicate regions where less than 80% of the models agree on the sign of the change and no overlay where at least 80% of the models agree on the sign of the change. Further details on data sources and processing are available in the chapter data table (Table 4.SM.1).

IPCC 2021, Chap. 4

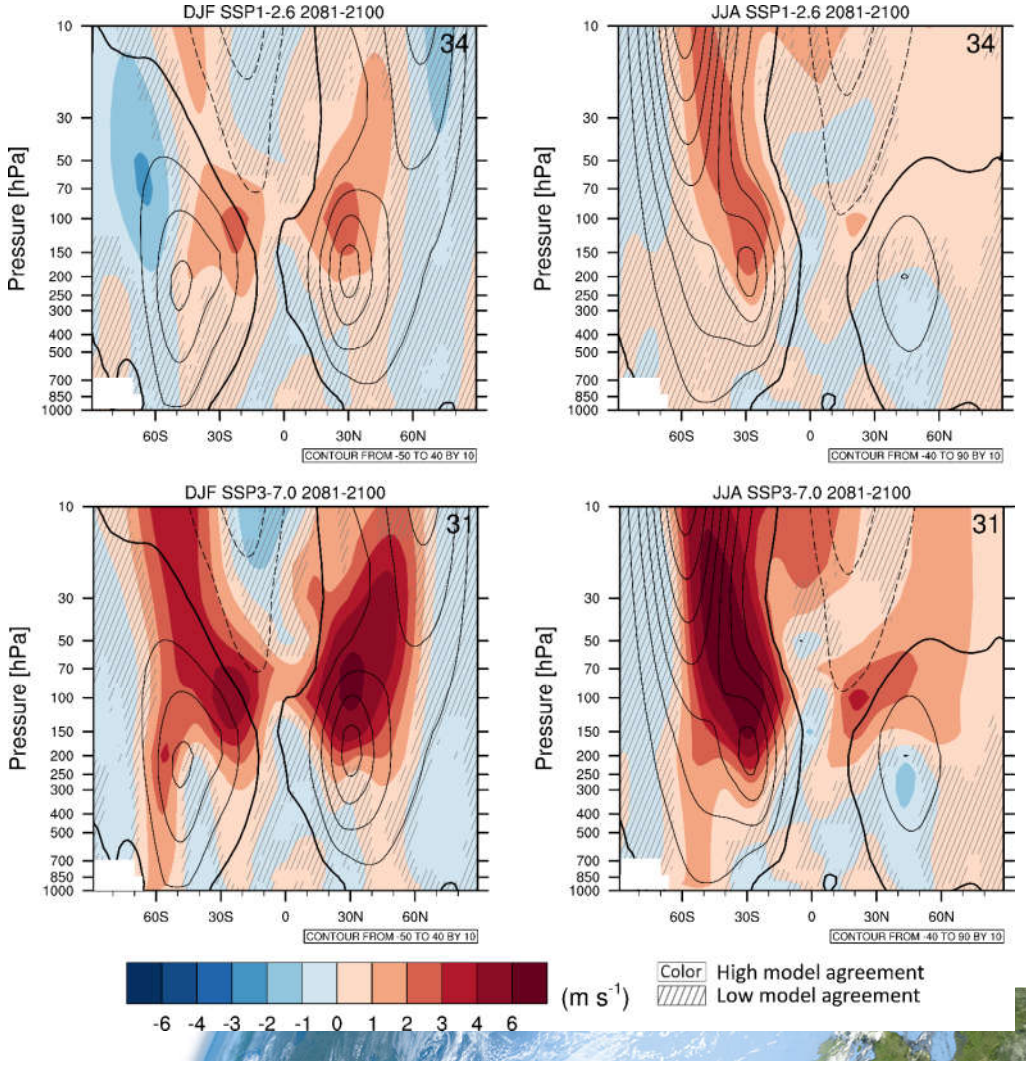
DJF SSP1-2.6 2081-2100
34
JJA SSP1-2.6 2081-2100
34
DJF SSP3-7.0 2081-2100
31
JJA SSP3-7.0 2081-2100
31
Pressure [hPa]
10
30
50
70
100
150
200
250
300
400
500
700
850
1000
60S
30S
0
30N
60N
CONTOUR FROM -50 TO 40 BY 10
CONTOUR FROM -40 TO 90 BY 10
-6 -4 -3 -2 -1 0 1 2 3 4 6
(m s-1)
Color High model agreement
Low model agreement

Changes in extratropical storm track density

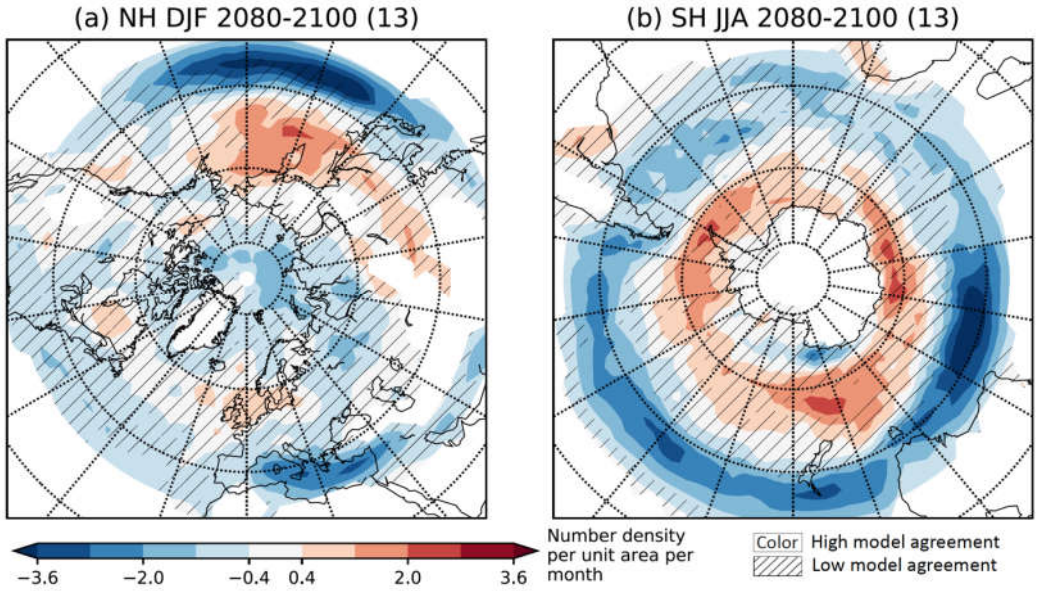

Figure 4.27: Changes in extratropical storm track density. Displayed are projected spatial pattern of multi-model mean change of extratropical storm track density in winter (NH DJF and SH JJA) in 2080–2100 for SSP5-8.5 relative to 1979–2014 based on 13 CMIP6 models. Diagonal lines indicate regions where fewer than 80% of the models agree on the sign of the change and no overlay where at least 80% of the models agree on the sign of change. Units are number density per 5 degree spherical cap per month. Further details on data sources and processing are available in the chapter data table (Table 4.SM.1).

Changes in extratropical storm track density

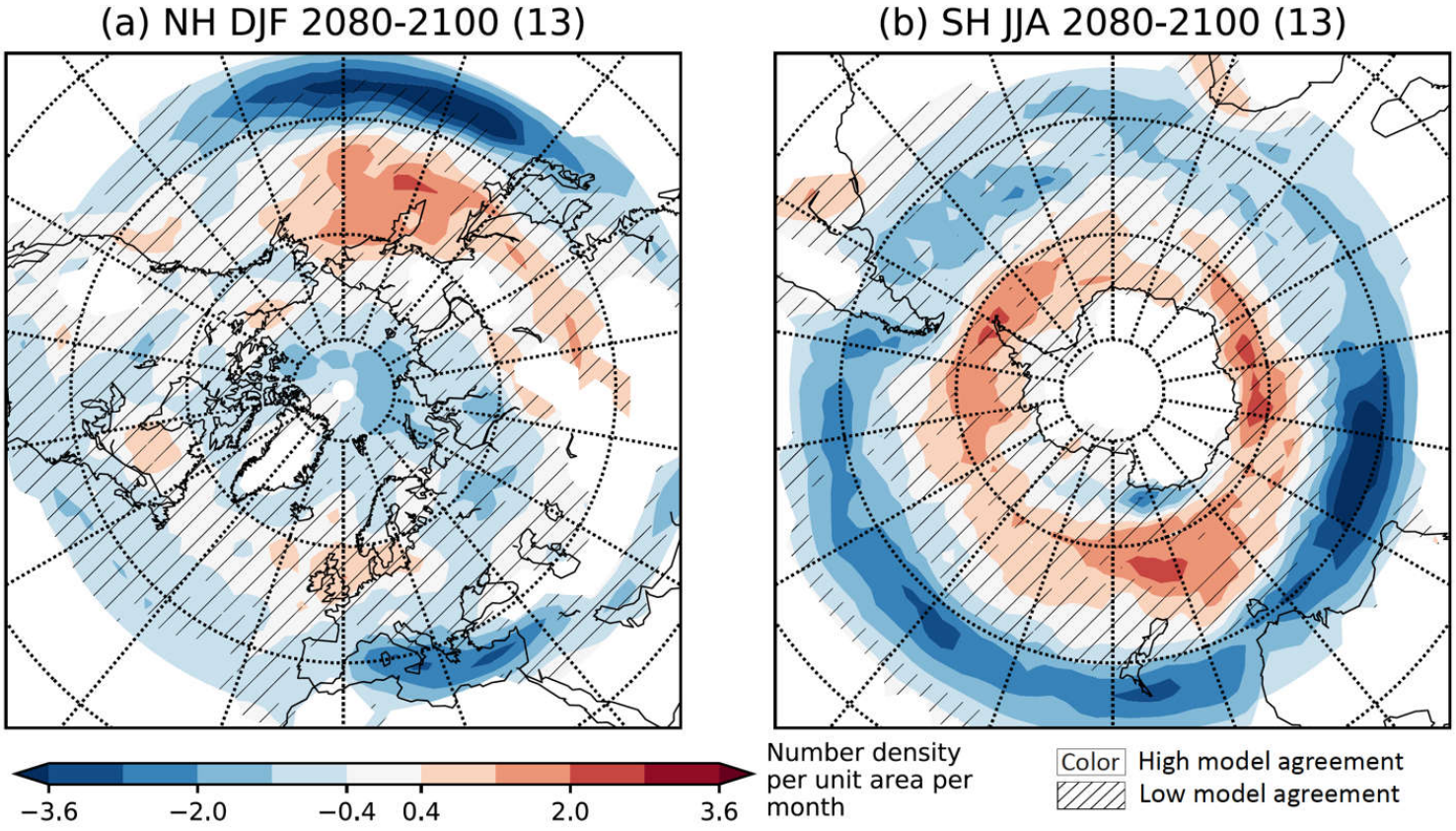

IPCC 2021, Chap. 4

Modes of variability (2)

Blocks in meteorology are large-scale patterns in the atmospheric pressure field that are nearly stationary, effectively "**blocking**" or redirecting migratory cyclones. They are also known as blocking highs or blocking anticyclones. These blocks can remain in place for several days or even weeks, causing the areas affected by them to have the same kind of weather for an extended period of time.

Projected wintertime atmospheric blocking frequencies

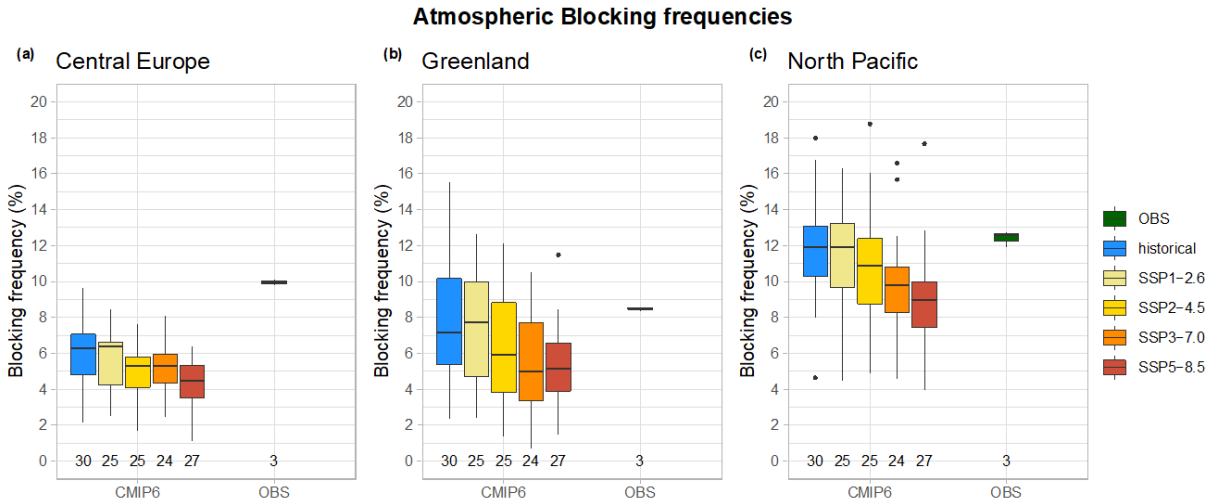

Figure 4.28: Projected wintertime atmospheric blocking frequencies. Box plot showing December-to-March atmospheric blocking frequencies from historical simulations over 1995–2014 and projections over 2081–2100, over (a) the Central European region (20°W–20°E, 45°N–65°N), (b) the Greenland region (65°W–20°W, 62.5°N–72.5°N), (c) the North Pacific region (130°E–150°W, 60°N–75°N). Values show the percentage of blocked days per season following the (Davini et al., 2012) index. Median values are the thick black horizontal bar. The lower whiskers extend from the first quartile to the smallest value in the ensemble, and the upper whiskers extend from the third quartile to the largest value. The whiskers are limited to an upper bound that is 1.5 times the interquartile range (the distance between the third and first quartiles). Black dots show outliers from the whiskers. The numbers below each bar report the number of models included. Observationally based values are obtained as the average of the ERA-Interim Reanalysis, the JRA-55 Reanalysis and the NCEP/NCAR Reanalysis. Adapted from (Davini and D'Andrea, 2020). Further details on data sources and processing are available in the chapter data table (Table 4.SM.1).

Projected wintertime atmospheric blocking frequencies

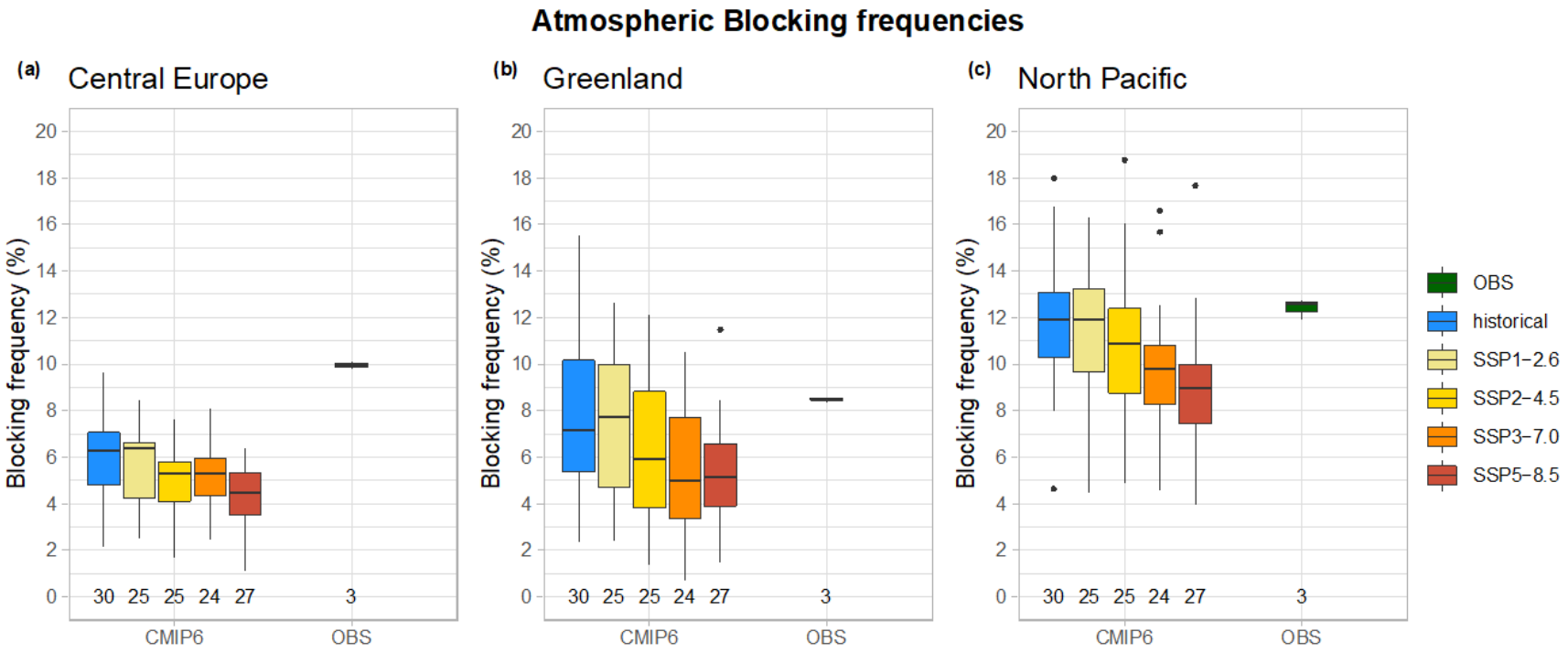

IPCC 2021, Chap. 4

Modes of variability (3)

The **Atlantic Multidecadal Oscillation (AMO)**, also known as **Atlantic Multidecadal Variability (AMV)**, is the theorized variability of the sea surface temperature (SST) of the North Atlantic Ocean on the timescale of several decades.

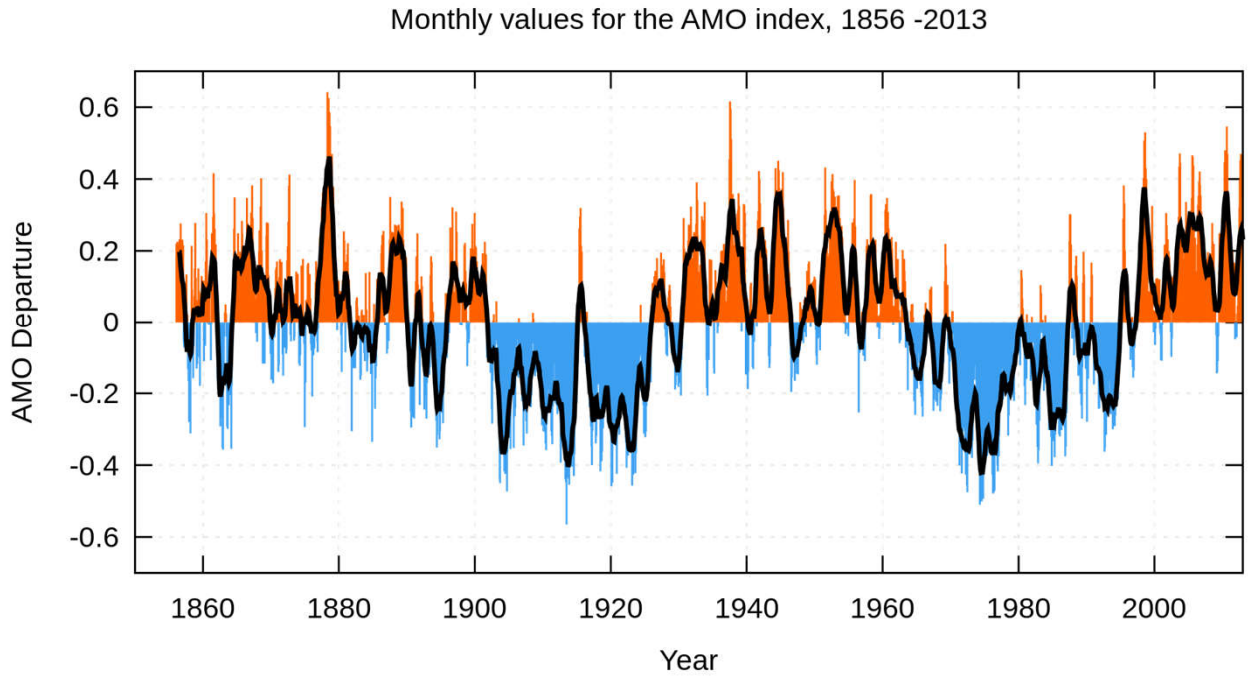

Statements in the Executive Summary

Large-scale Circulation and Modes of Variability (3)

Near-term predictions and projections of the sub-polar branch of the Atlantic Multi-decadal Variability (AMV) on the decadal timescale have improved in CMP6 models compared to CMIP5 (*high confidence*). This is likely to be related to a more accurate response to natural forcing in CMIP6 models. Initialization contributes to the reduction of uncertainty and to predicting subpolar sea surface temperature. AMV influences on the nearby regions can be predicted over lead times of 5–8 years (*medium confidence*). {4.4.3}

IPCC 2021, Chap. 4

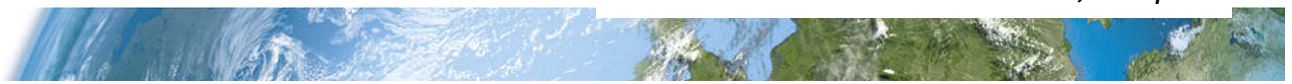

Modes of variability (4)

El Niño–Southern Oscillation (ENSO) is an irregular periodic variation in winds and sea surface temperatures over the tropical eastern Pacific Ocean, affecting the climate of much of the tropics and subtropics. The warming phase of the sea temperature is known as El Niño and the cooling phase as La Niña.

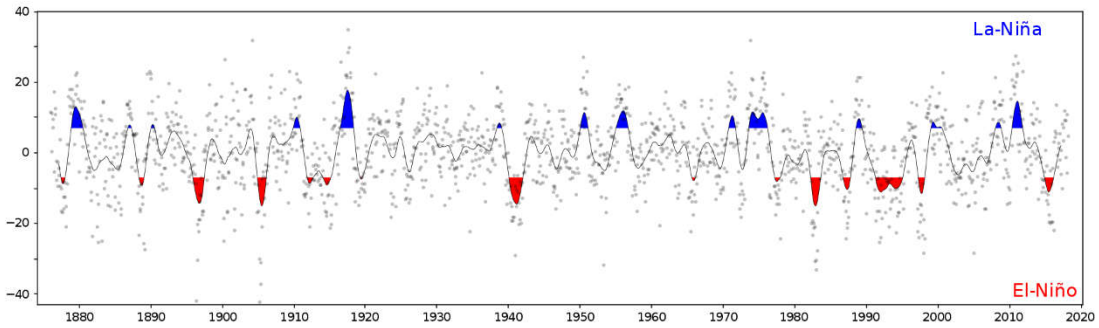

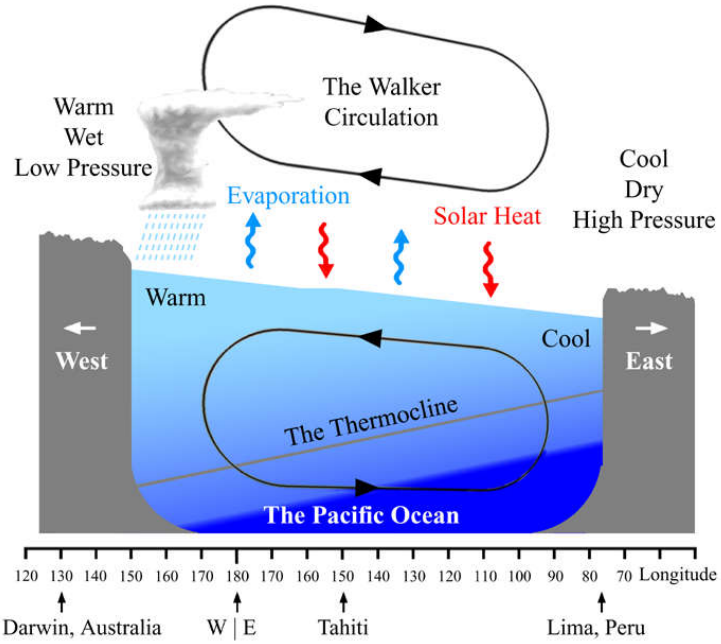

Statements in the Executive Summary

Large-scale Circulation and Modes of Variability (3)

Near-term predictions and projections of the sub-polar branch of the Atlantic Multi-decadal Variability (AMV) on the decadal timescale have improved in CMP6 models compared to CMIP5 (*high confidence*). This is likely to be related to a more accurate response to natural forcing in CMIP6 models. Initialization contributes to the reduction of uncertainty and to predicting subpolar sea surface temperature. AMV influences on the nearby regions can be predicted over lead times of 5–8 years (*medium confidence*). {4.4.3}

It is *virtually certain* that the El Niño–Southern Oscillation (ENSO) will remain the dominant mode of interannual variability in a warmer world. There is no model consensus for a systematic change in intensity of ENSO sea surface temperature (SST) variability over the 21st century in any of the SSP scenarios assessed (*medium confidence*). However, it is *very likely* that ENSO rainfall variability, used for defining extreme El Niños and La Niñas, will increase significantly, regardless of amplitude changes in ENSO SST variability, by the second half of the 21st century in scenarios SSP2-4.5, SSP3-7.0, and SSP5-8.5. {4.3.3, 4.5.3, 8.4.2}

IPCC 2021, Chap. 4

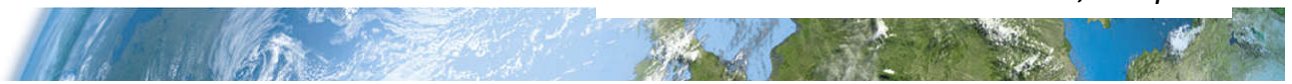

Statements in the Executive Summary

Cryosphere and Ocean (1)

Under the SSP2-4.5, SSP3-7.0, and SSP5-8.5 scenarios, it is *likely* that the Arctic Ocean in September, the month of annual minimum sea ice area, will become practically ice-free (sea ice area less than 1 million km^2) averaged over 2081–2100 and all available simulations. Arctic sea ice area in March, the month of annual maximum sea ice area, also decreases in the future under each of the considered scenarios, but to a much lesser degree (in percentage terms) than in September (*high confidence*). {4.3.2}

IPCC 2021, Chap. 4

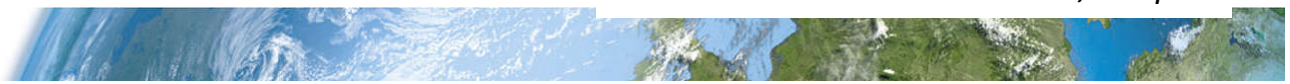

Selected indicators of global climate change from CMIP6 historical and scenario simulations

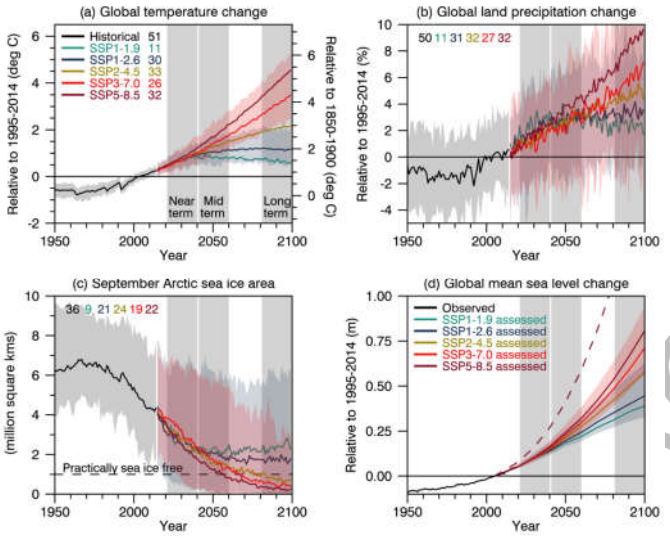

Figure 4.2: **Selected indicators of global climate change from CMIP6 historical and scenario simulations.** (a) Global surface air temperature changes relative to the 1995–2014 average (left axis) and relative to the 1850–1900 average (right axis; offset by 0.82°C, which is the multi-model mean and close to observed best estimate, Cross-Chapter Box 2.1, Table 1). (b) Global land precipitation changes relative to the 1995–2014 average. (c) September Arctic sea-ice area. (d) Global mean sea-level change (GMSL) relative to the 1995–2014 average. (a), (b) and (d) are annual averages, (c) are September averages. In (a)-(c), the curves show averages over the CMIP6 simulations, the shadings around the SSP1-2.6 and SSP3-7.0 curves show 5–95% ranges, and the numbers near the top show the number of model simulations used. Results are derived from concentration-driven simulations. In (d), the barystatic contribution to GMSL (i.e., the contribution from land-ice melt) has been added offline to the CMIP6 simulated contributions from thermal expansion (thermosteric). The shadings around the SSP1-2.6 and SSP3-7.0 curves show 5–95% ranges. The dashed curve is the *low confidence* and low likelihood outcome at the high end of SSP5-8.5 and reflects deep uncertainties arising from potential ice-sheet and ice-cliff instabilities. This curve at year 2100 indicates 1.7 m of GMSL rise relative to 1995–2014. More information on the calculation of GMSL are available in Chapter 9, and further regional details are provided in the Atlas. Further details on data sources and processing are available in the chapter data table (Table 4.SM.1).

IPCC 2021, Chap. 4

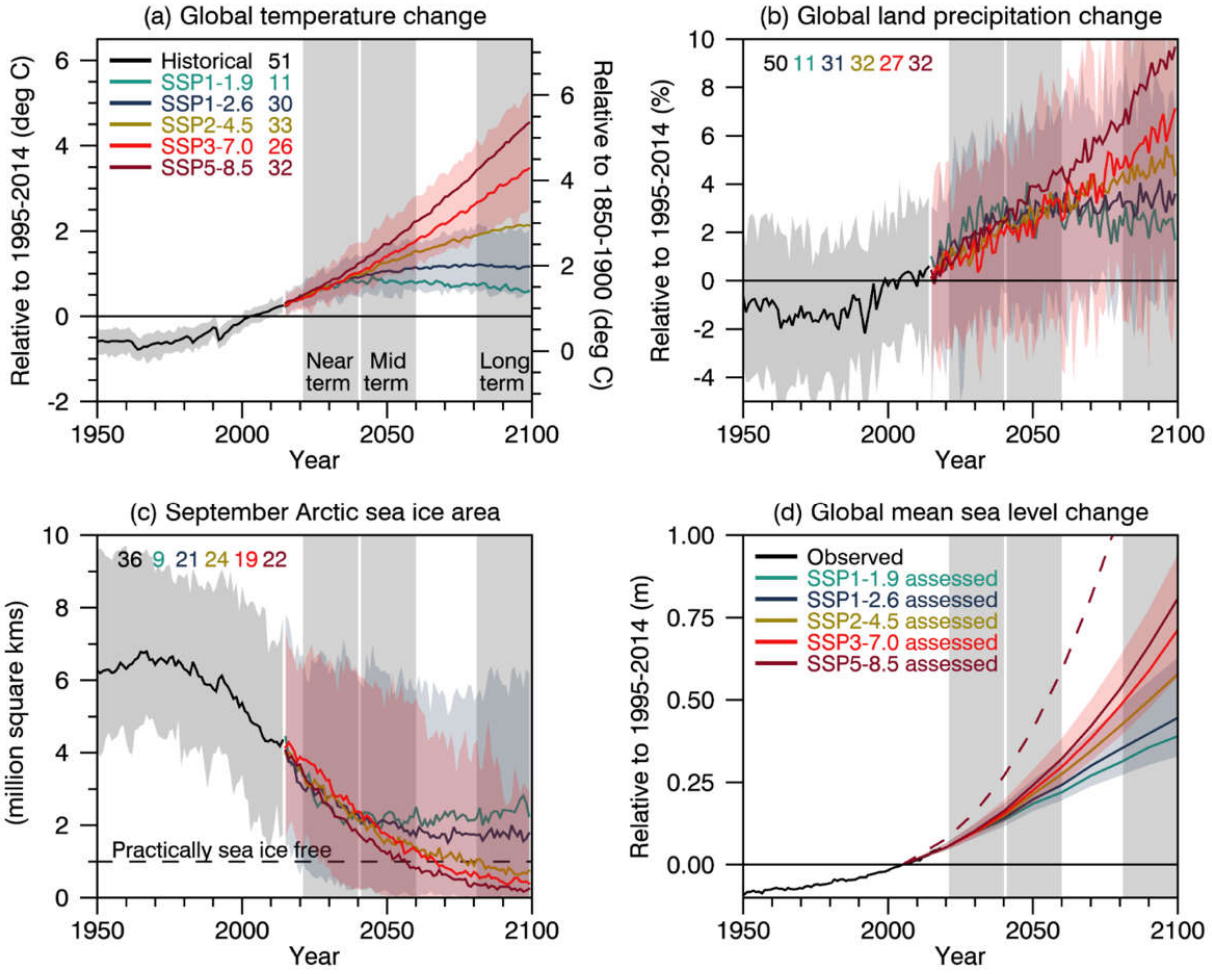

IPCC 2021, Chap. 4

Statements in the Executive Summary

Cryosphere and Ocean (1)

Under the SSP2-4.5, SSP3-7.0, and SSP5-8.5 scenarios, it is *likely* that the Arctic Ocean in September, the month of annual minimum sea ice area, will become practically ice-free (sea ice area less than 1 million km^2) averaged over 2081–2100 and all available simulations. Arctic sea ice area in March, the month of annual maximum sea ice area, also decreases in the future under each of the considered scenarios, but to a much lesser degree (in percentage terms) than in September (*high confidence*). {4.3.2}

Under the five scenarios assessed, it is *virtually certain* that global mean sea level (GMSL) will continue to rise through the 21st century. For the period 2081–2100 relative to 1995–2014, GMSL is *likely* to rise by 0.46–0.74 m under SSP3-7.0 and by 0.30–0.54 m under SSP1-2.6 (*medium confidence*). For the assessment of change in GMSL, the contribution from land-ice melt has been added offline to the CMIP6-simulated contributions from thermal expansion. {4.3.2. 9.6}

IPCC 2021, Chap. 4

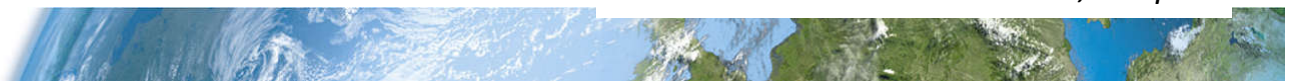

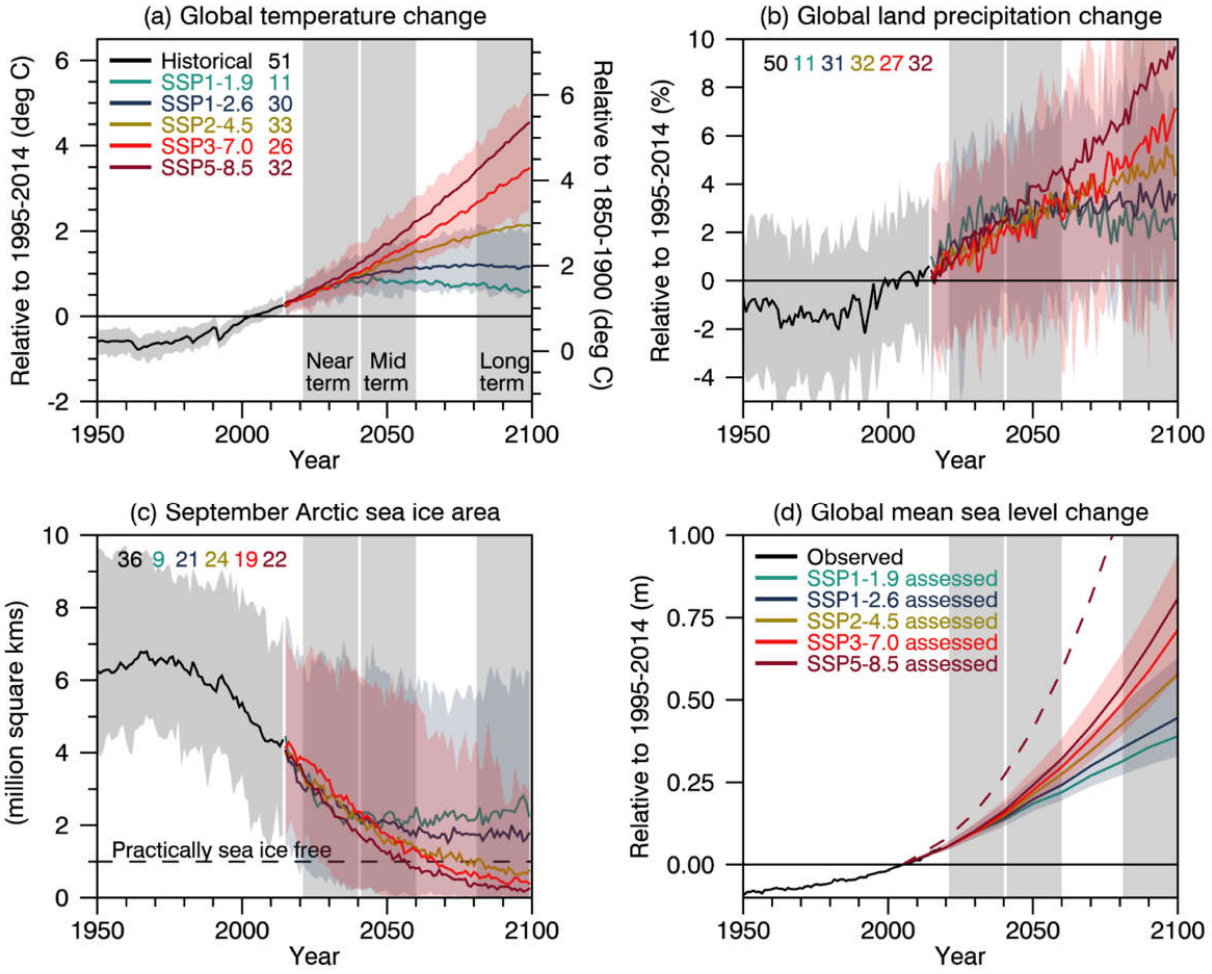

IPCC 2021, Chap. 4

Statements in the Executive Summary

Cryosphere and Ocean (2)

It is *very likely* that the cumulative uptake of carbon by the ocean and by land will increase through to the end of the 21st century. Carbon uptake by land shows greater increases but with greater uncertainties than for ocean carbon uptake. The fraction of emissions absorbed by land and ocean sinks will be smaller under high emission scenarios than under low emission scenarios (*high confidence*). Ocean surface pH will decrease steadily through the 21st century, except for SSP1-1.9 and SSP1-2.6 where values decrease until around 2070 and then increase slightly to 2100 (high confidence). {4.3.2, 5.4}

IPCC 2021, Chap. 4

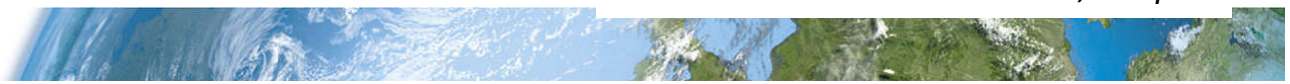

Long-term change of annual and zonal ocean pH

Figure 4.29: Long-term change of annual and zonal ocean pH. Displayed are multi-model mean change in annual and zonal ocean pH in 2081–2100 relative to the mean of 1995–2014 for SSP1-2.6 and SSP3-7.0, respectively. Eleven CMIP6 model results are used. Diagonal lines indicate regions where fewer than 80% of the models agree on the sign of the change and no overlay where at least 80% of the models agree on the sign of change. Further details on data sources and processing are available in the chapter data table (Table 4.SM.1).

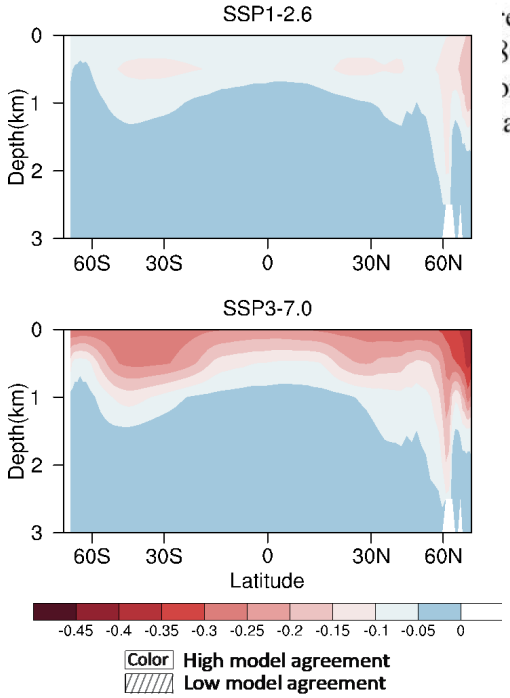

IPCC 2021, Chap. 4

Long-term change of annual and zonal ocean pH

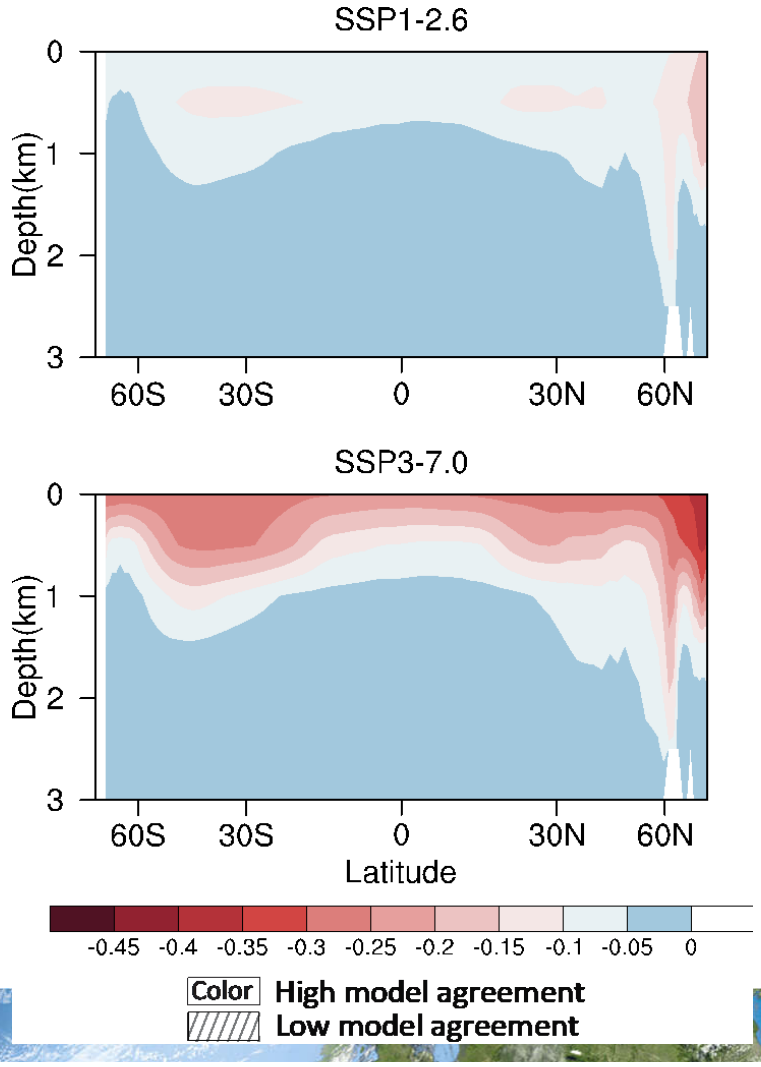

IPCC 2021, Chap. 4

Statements in the Executive Summary

Climate Response to Emission Reduction, Carbon Dioxide Removal, and Solar Radiation Modification (1)

If strong mitigation is applied from 2020 onward as reflected in SSP1-1.9, its effect on 20-year trends in GSAT would likely emerge during the near term (2021–2040), measured against an assumed non-mitigation scenario such as SSP3-7.0 and SSP5-8.5. However, the response of many other climate quantities to mitigation would be largely masked by internal variability during the near term, especially on the regional scale (*high confidence*). The mitigation benefits for these quantities would emerge only later during the 21st century (*high confidence*). During the near term, a small fraction of the surface can show cooling under all scenarios assessed here, so near-term cooling at any given location is fully consistent with GSAT increase (*high confidence*). Events of reduced and increased GSAT trends at decadal timescales will continue to occur in the 21st century but will not affect the centennial warming (*very high confidence*). {4.6.3, Cross-Chapter Box 3.1}

IPCC 2021, Chap. 4

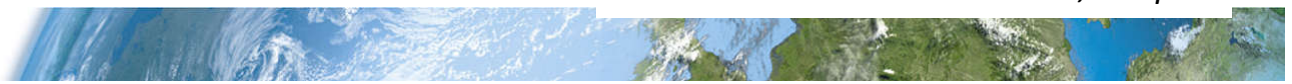

Statements in the Executive Summary

Climate Response to Emission Reduction, Carbon Dioxide Removal, and Solar Radiation Modification (2)

Because of the near-linear relationship between cumulative carbon emissions and GSAT change, the cooling or avoided warming from carbon dioxide removal (CDR) is proportional to the cumulative amount of CO_2 removed by CDR (*high confidence*). The climate system response to net negative CO_2 emissions is expected to be delayed by years to centuries. Net negative CO_2 emissions due to CDR will not reverse some climate change, such as sea level rise, at least for several centuries (*high confidence*). The climate effect of a sudden and sustained CDR termination would depend on the amount of CDR-induced cooling prior to termination and the rate of background CO_2 emissions at the time of termination (*high confidence*). {4.6.3, 5.5, 5.6}

IPCC 2021, Chap. 4

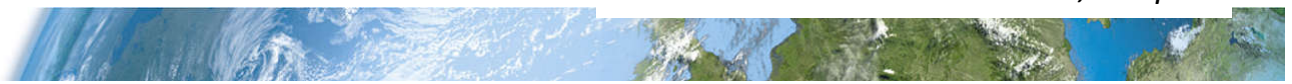

Delayed climate response to CDR-caused net negative CO_2 emissions

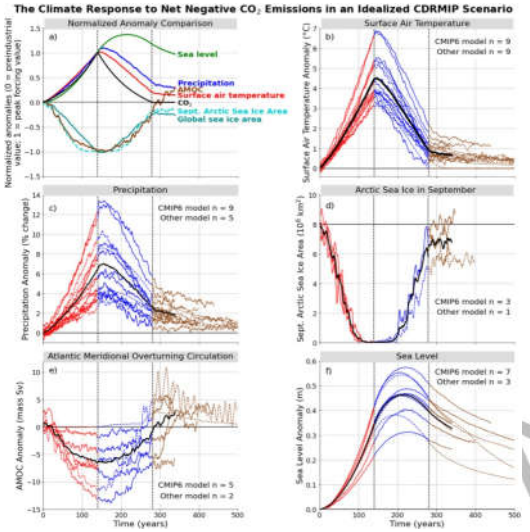

Figure 4.37: Delayed climate response to CDR-caused net negative CO_2 emissions. Multi-model simulated response in global and annual mean climate variables for a ramp-up followed by ramp-down of CO_2. Atmospheric CO_2 increases from the pre-industrial level at a rate of 1% yr^{-1} to 4×CO_2, then decreases at the same rate to the pre-industrial level and then remains constant. The ramp-down phase represents the period of net negative CO_2 emissions. a) normalized ensemble mean anomaly of key variables as a function of year, including atmospheric CO_2, surface air temperature, precipitation, thermosteric sea-level rise (see Glossary), global sea-ice area, Northern Hemisphere sea-ice area in September, and Atlantic meridional overturning circulation (AMOC); b) surface air temperature; c) precipitation; d) September Arctic sea-ice area; e) AMOC; f) thermostatic sea level; 5-year running means are shown for all variables except the sea-level rise. In b–f, red lines represent the phase of CO_2 ramp-up, blue lines represent the phase of CO_2 ramp-down, brown lines represent the period after CO_2 has returned to pre-industrial level, and black lines represent the multi-model mean. For all of the segments in b–f, the solid coloured lines are CMIP6 models, and the dashed lines are other models (i.e., EMICs, CMIP5 era models). Vertical dashed lines indicate peak CO_2 and when CO_2 again reaches pre-industrial value. The number of CMIP6 and non-CMIP6 models used is indicated in each panel. The time series for the multi-model means (b–f) and the normalized anomalies (a) are terminated when data from all models are not available, in order to avoid the discontinuity in the time series. Further details on data sources and processing are available in the chapter data table (Table 4.SM.1).

IPCC 2021, Chap. 4

Delayed climate response to CDR-caused net negative CO_2 emissions

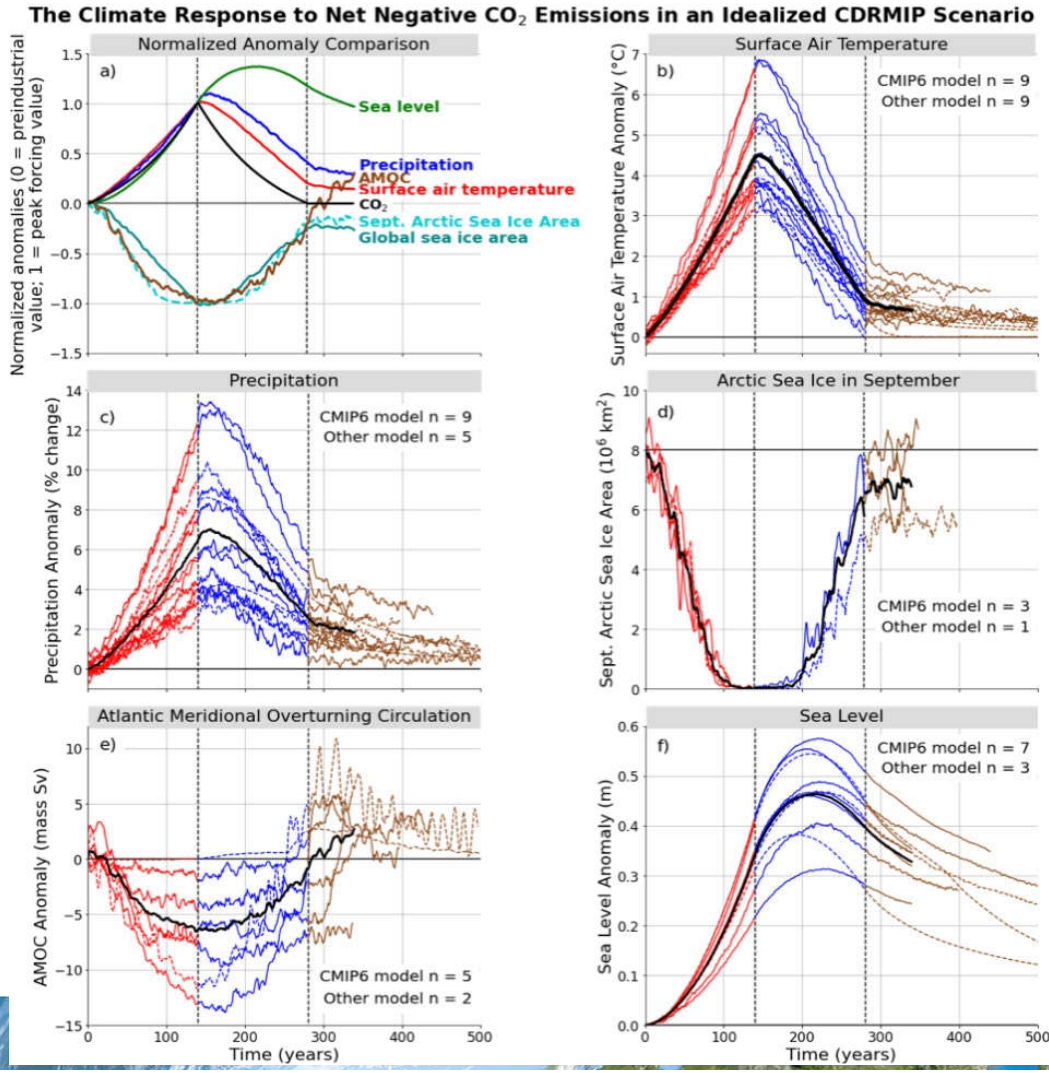

IPCC 2021, Chap. 4

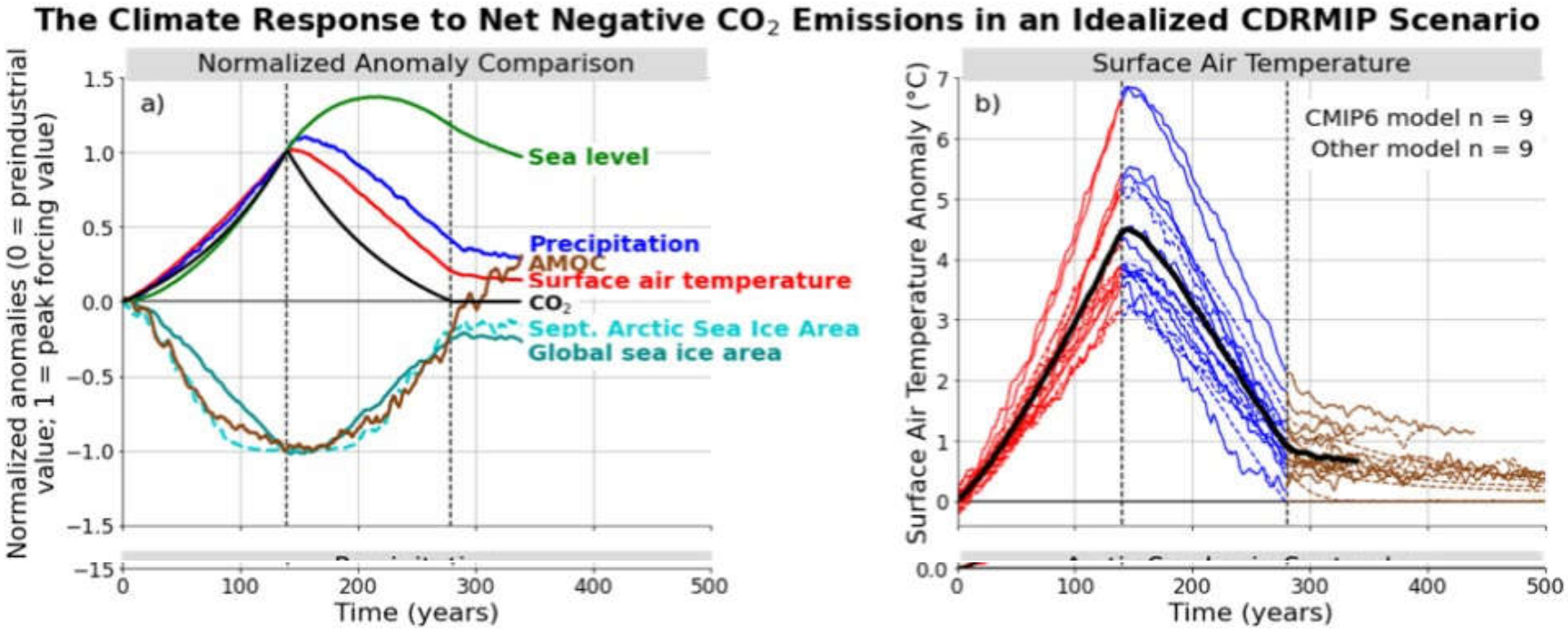

IPCC 2021, Chap. 4

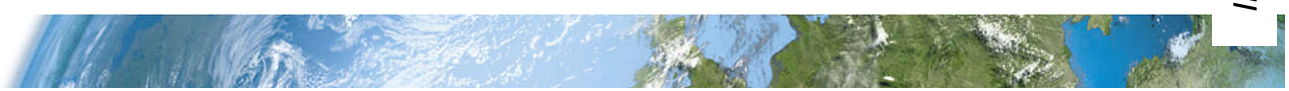

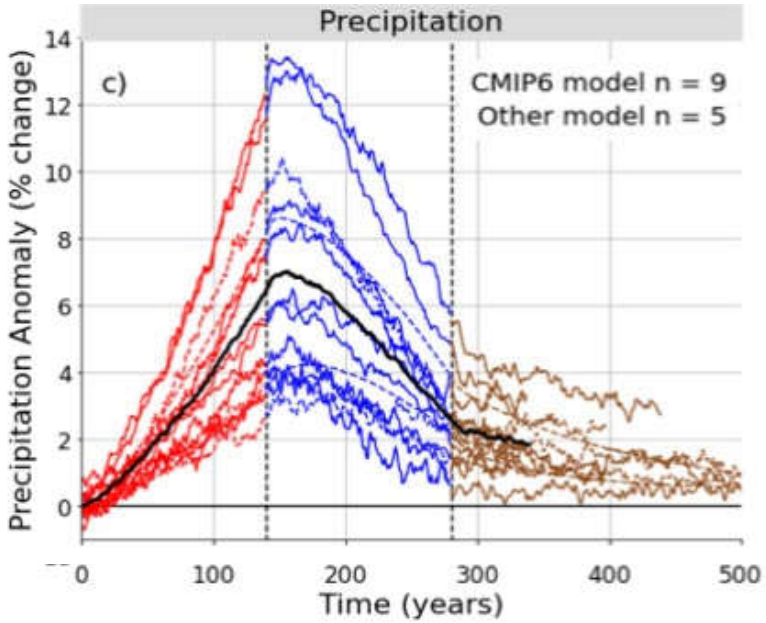

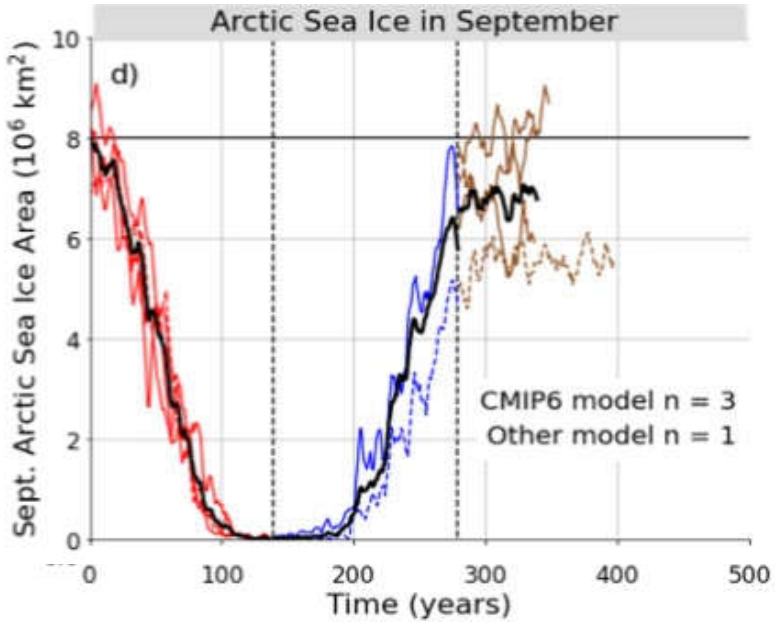

IPCC 2021, Chap. 4

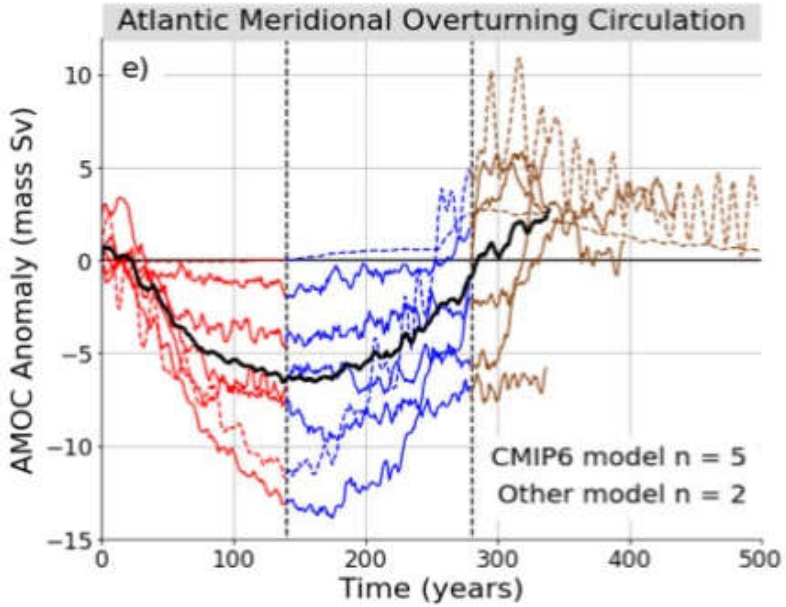

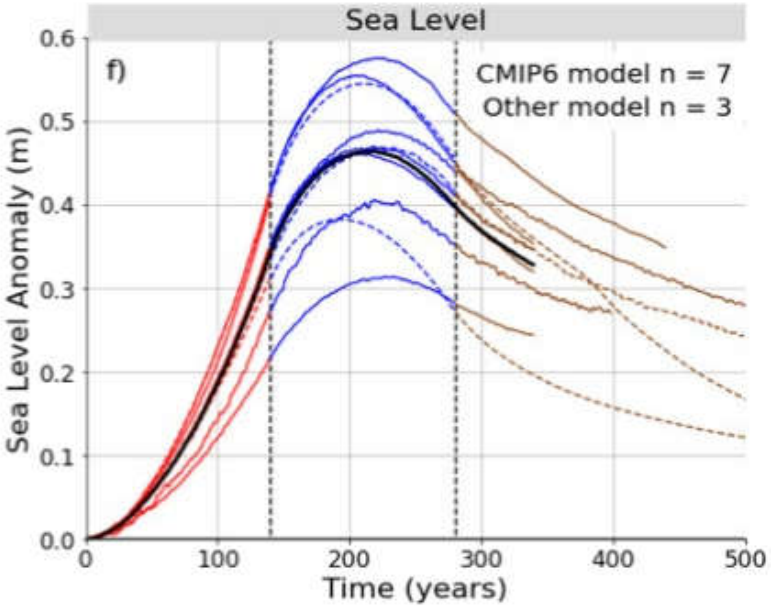

IPCC 2021, Chap. 4

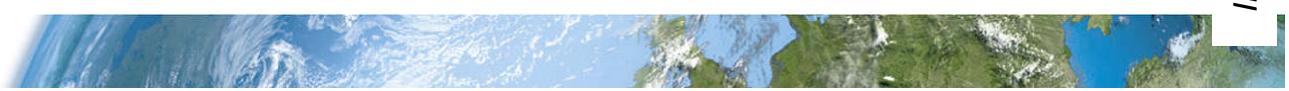

Statements in the Executive Summary

Climate Response to Emission Reduction, Carbon Dioxide Removal, and Solar Radiation Modification (3)

Solar radiation modification (SRM) could offset some of the effects of anthropogenic warming on global and regional climate, but there would be substantial residual and overcompensating climate change at the regional scale and seasonal timescale (*high confidence*), and there is *low confidence* in our understanding of the climate response to SRM, specifically at the regional scale. Since the AR5, understanding of the global and regional climate response to SRM has improved, due to modelling work with more sophisticated treatment of aerosol-based SRM options and stratospheric processes. Improved modelling suggests that multiple climate goals could be met simultaneously. A sudden and sustained termination of SRM in a high-emission scenario such as SSP5-8.5 would cause a rapid climate change (*high confidence*). However, a gradual phase-out of SRM combined with emissions reductions and CDR would *more likely than* not avoid larger rates of warming. {4.6.3}

IPCC 2021, Chap. 4

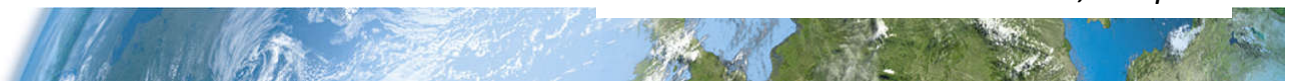

Multi-model response per degree global mean cooling in temperature and precipitation in response to CO_2 forcing and SRM forcing

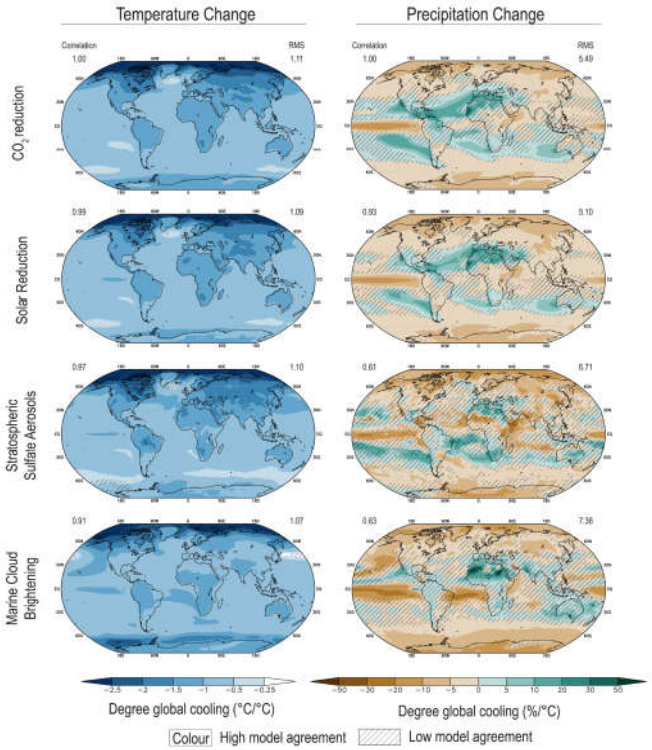

Figure 4.38: Multi-model response per degree global mean cooling in temperature and precipitation in response to CO_2 forcing and SRM forcing. Top row shows the response to a CO_2 decrease, calculated as the difference between pre-industrial control simulation and abrupt4 • CO_2 simulations where the CO_2 concentration is quadrupled abruptly from the pre-industrial level (11-model average); second row shows the response to a globally uniform solar reduction, calculated as the difference between GeoMIP experiment G1 and abrupt4 • CO_2 (11-model average); third row shows the response to stratospheric sulphate aerosol injection, calculated as the difference between GeoMIP experiment G4 (a continuous injection of 5Tg SO_2 per year at one point on the equator into the lower stratosphere against the RCP4.5 background scenario) and RCP4.5 (6-model average); and bottom row shows the response to marine cloud brightening, calculated as the difference between GeoMIP experiment G4cdnc (increase cloud droplet concentration number in marine low cloud by 50% over the global ocean against RCP4.5 background scenario) and RCP4.5 (8-model average). All differences (average of years 11–50 of simulation) are normalized by the global mean cooling in each scenario, averaged over years 11–50. Diagonal lines represent regions where fewer than 80% of the models agree on the sign of change. The values of correlation represent the spatial correlation of each SRM-induced temperature and precipitation change pattern with the pattern of change caused by a reduction of atmospheric CO_2. RMS (root mean square) is calculated based on the fields shown in the maps (normalized by global mean cooling). Further details on data sources and processing are available in the chapter data table (Table 4.SM.1).

IPCC 2021, Chap. 4

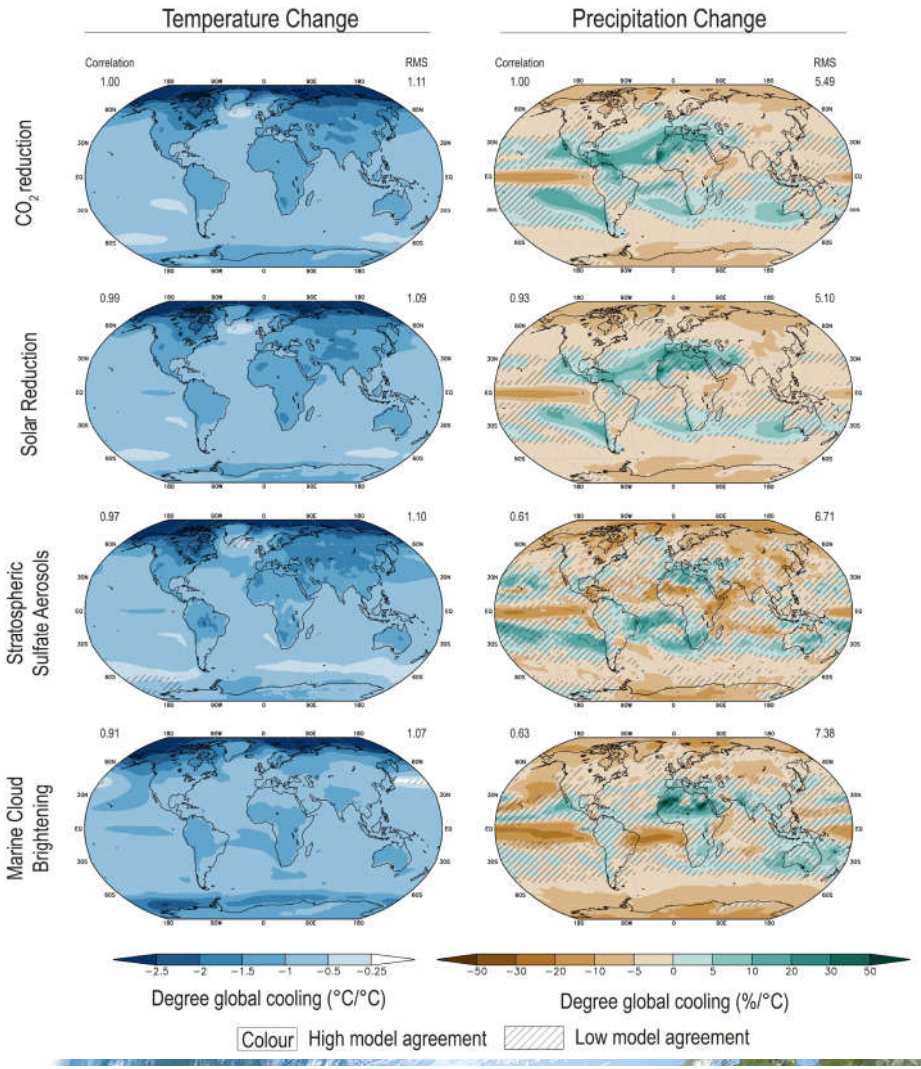

IPCC 2021, Chap. 4

Statements in the Executive Summary

Climate Change Commitment and Change Beyond 2100 (1)

Earth system modelling experiments since AR5 confirm that the zero CO_2 emissions commitment (the additional rise in GSAT after all CO_2 emissions cease) is small (*likely* less than 0.3°C in magnitude) on decadal time scales, but that it may be positive or negative. There is *low confidence* in the sign of the zero CO_2 emissions commitment. Consistent with SR1.5, the central estimate is taken as zero for assessments of remaining carbon budgets for global warming levels of 1.5°C or 2°C. {4.7.2, 5.5.2}.

IPCC 2021, Chap. 4

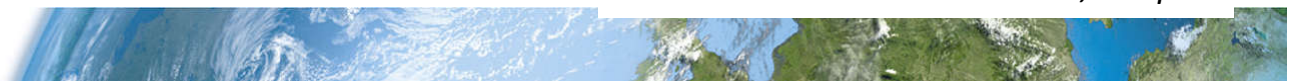

Zero Emissions Commitment (ZEC)

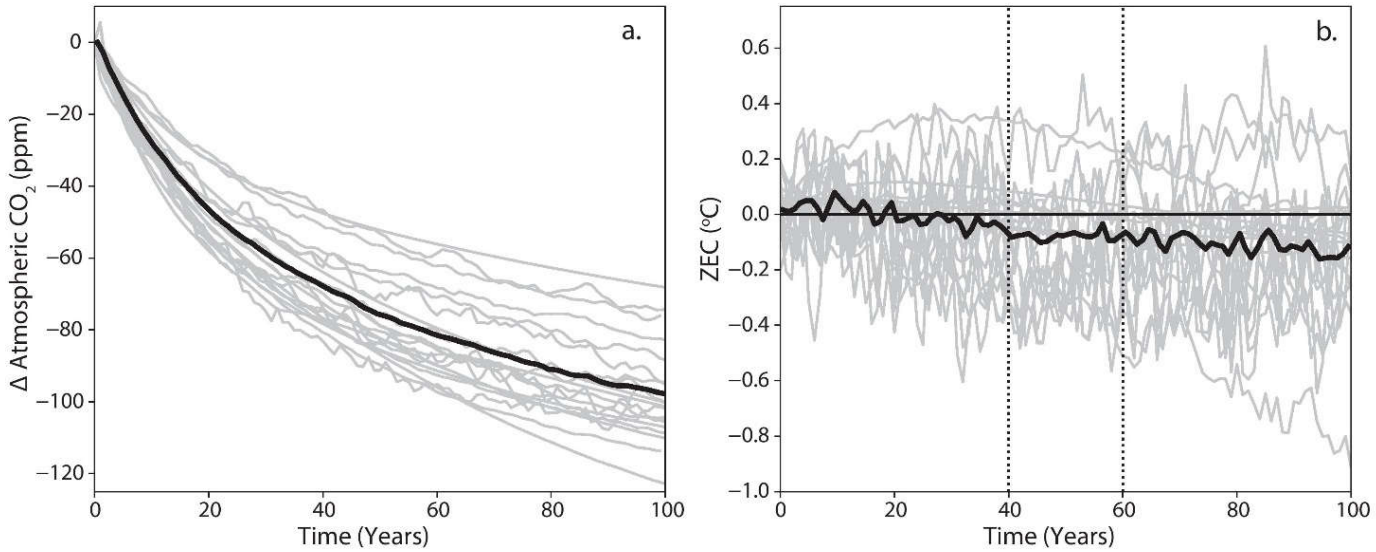

Figure 4.39: Zero Emissions Commitment (ZEC). Changes in (a) atmospheric CO_2 concentration and (b) evolution of GSAT following cessation of CO_2 emissions branched from the 1% per year experiment after emission of 1000 PgC (Jones et al., 2019). ZEC is the temperature anomaly relative to the estimated temperature at the year of cessation. ZEC_{50} is the 20-year mean GSAT change centred on 50 years after the time of cessation (see Table 4.8) – this period is marked with the vertical dotted lines. Multi-model mean is shown as thick black line, individual model simulations are in grey. Further details on data sources and processing are available in the chapter data table (Table 4.SM.1).

IPCC 2021, Chap. 4

Zero Emissions Commitment (ZEC)

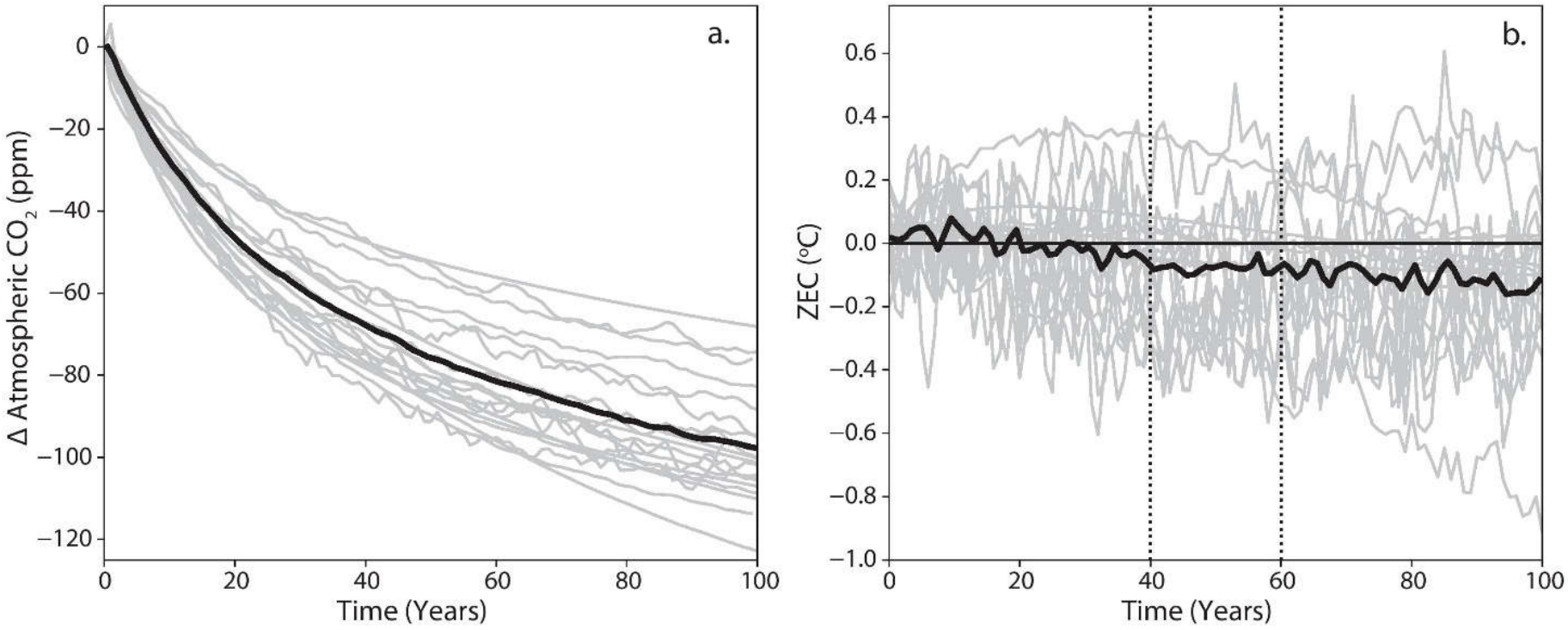

IPCC 2021, Chap. 4

Statements in the Executive Summary

Climate Change Commitment and Change Beyond 2100 (1)

Earth system modelling experiments since AR5 confirm that the zero CO_2 emissions commitment (the additional rise in GSAT after all CO_2 emissions cease) is small (*likely* less than 0.3°C in magnitude) on decadal time scales, but that it may be positive or negative. There is *low confidence* in the sign of the zero CO_2 emissions commitment. Consistent with SR1.5, the central estimate is taken as zero for assessments of remaining carbon budgets for global warming levels of 1.5°C or 2°C. {4.7.2, 5.5.2}.

Overshooting specific global warming levels such as 2°C has effects on the climate system that persist beyond 2100 *(medium confidence*). Under one scenario including a peak and decline in atmospheric CO_2 concentration (SSP5-3.4-OS), some climate metrics such as GSAT begin to decline but do not fully reverse by 2100 to levels prior to the CO_2 peak (*medium confidence*). GMSL continues to rise in all models up to 2100 despite a reduction in CO_2 to 2040 levels. {4.6.3, 4.7.1, 4.7.2}

IPCC 2021, Chap. 4

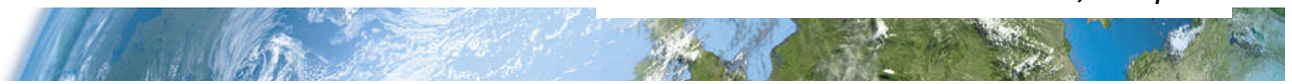

Statements in the Executive Summary

Climate Change Commitment and Change Beyond 2100 (2)

Using extended scenarios beyond 2100, projections show *likely* warming by 2300, relative to 1850−1900, of 1.0°C−2.2°C for SSP1-2.6 and 6.6°C−14.1°C for SSP5-8.5. By 2300, warming under the SSP5-3.4-OS overshoot scenario decreases from a peak around year 2060 to a level very similar to SSP1-2.6. Precipitation over land continues to increase strongly under SSP5-8.5. GSAT projected for the end of the 23rd century under SSP2-4.5 (2.3−4.6°C) has not been experienced since the mid-Pliocene, about 3 million years ago. GSAT projected for the end of the 23rd century under SSP5-8.5 (6.6−14.1°C) overlaps with the range estimated for the Miocene Climatic Optimum (5°C−10°C) and Early Eocene Climatic Optimum (10°C−18°C), about 15 and 50 million years ago, respectively (*medium confidence*). {2.3.1.1, 4.7.1}

IPCC 2021, Chap. 4

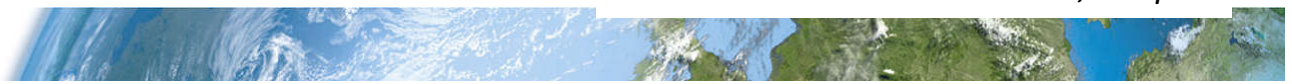

Simulated climate changes up to 2300 under the extended SSP scenarios

Figure 4.40: Simulated climate changes up to 2300 under the extended SSP scenarios. Displayed are (a) projected GSAT change, relative to 1850–1900, from CMIP6 models (individual lines) and MAGICC7 (shaded plumes), (b) as (a) but zoomed in to show low-emission scenarios, (c) global land precipitation change, and (d) September Arctic sea-ice area. Further details on data sources and processing are available in the chapter data table (Table 4.SM.1).

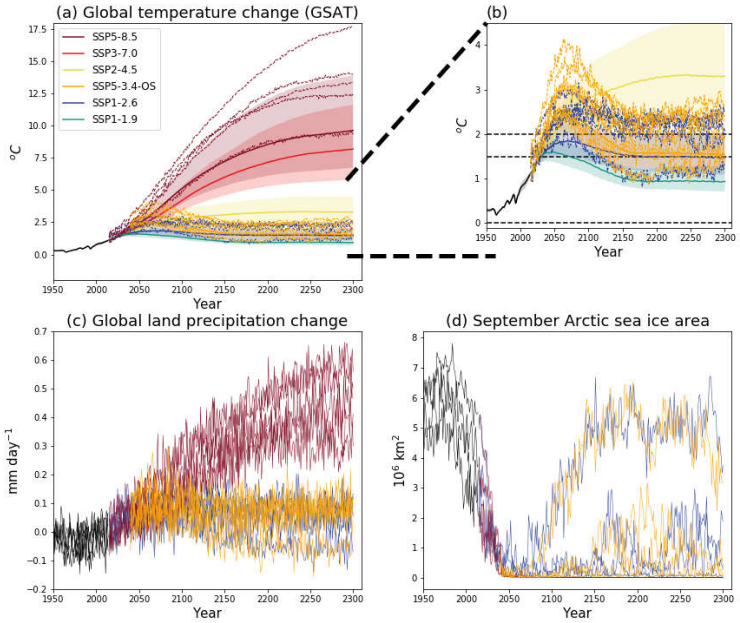

IPCC 2021, Chap. 4

Simulated climate changes up to 2300 under the extended SSP scenarios

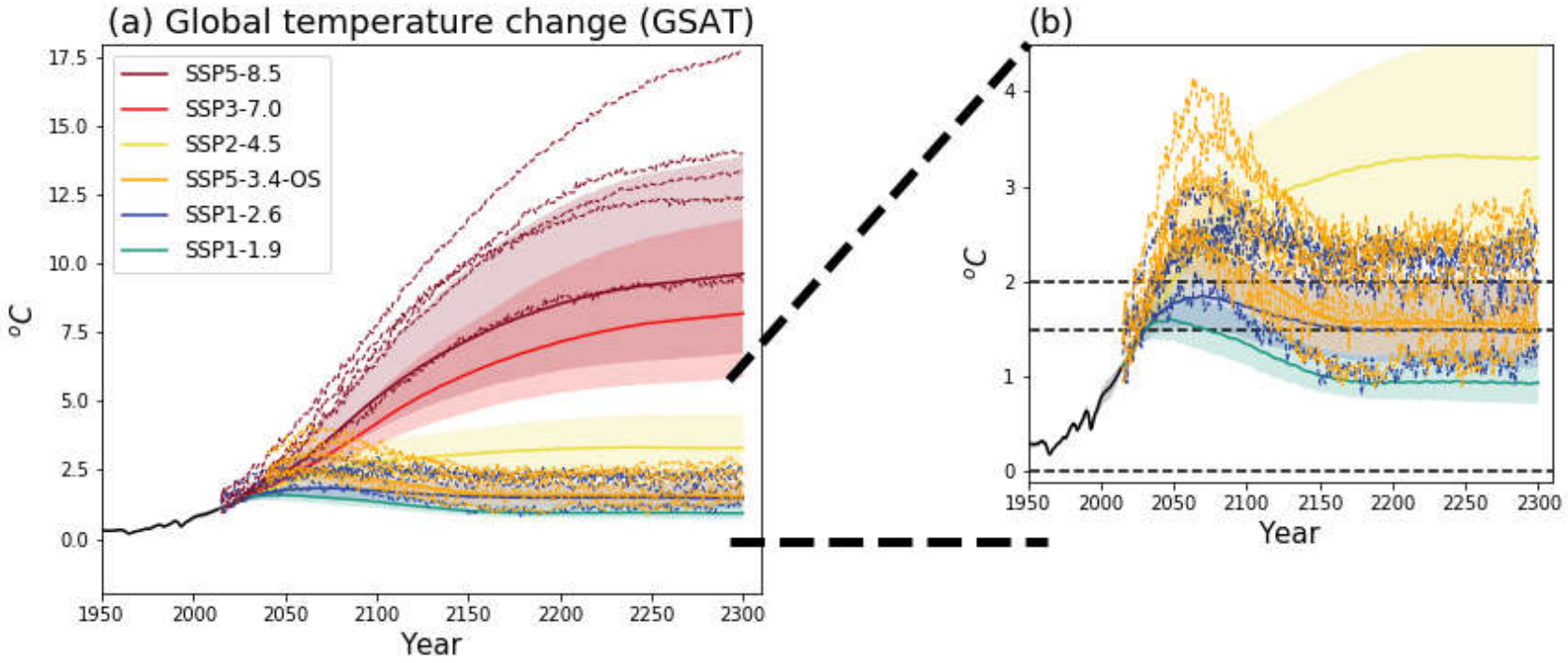

IPCC 2021, Chap. 4

Simulated climate changes up to 2300 under the extended SSP scenarios

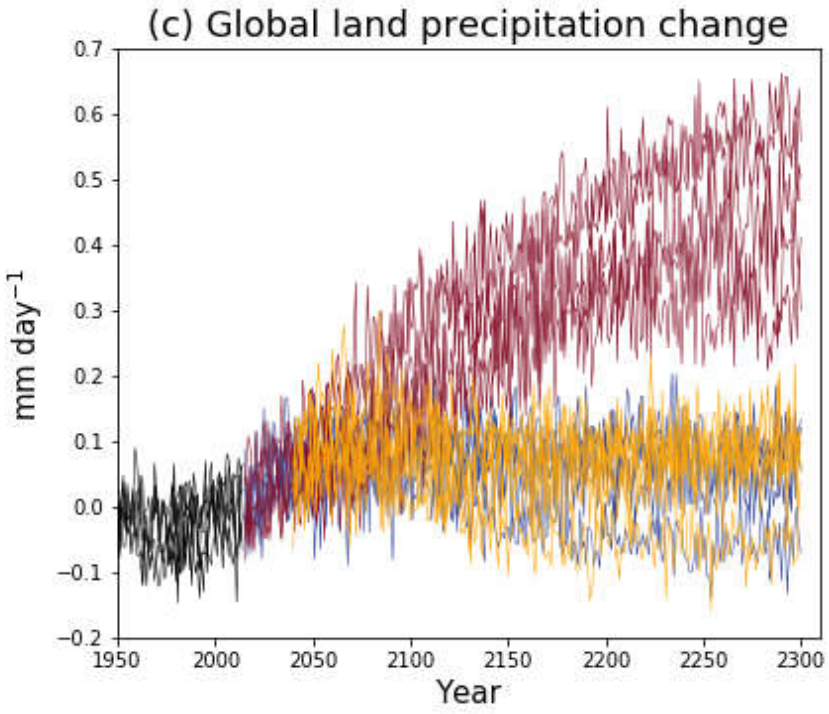

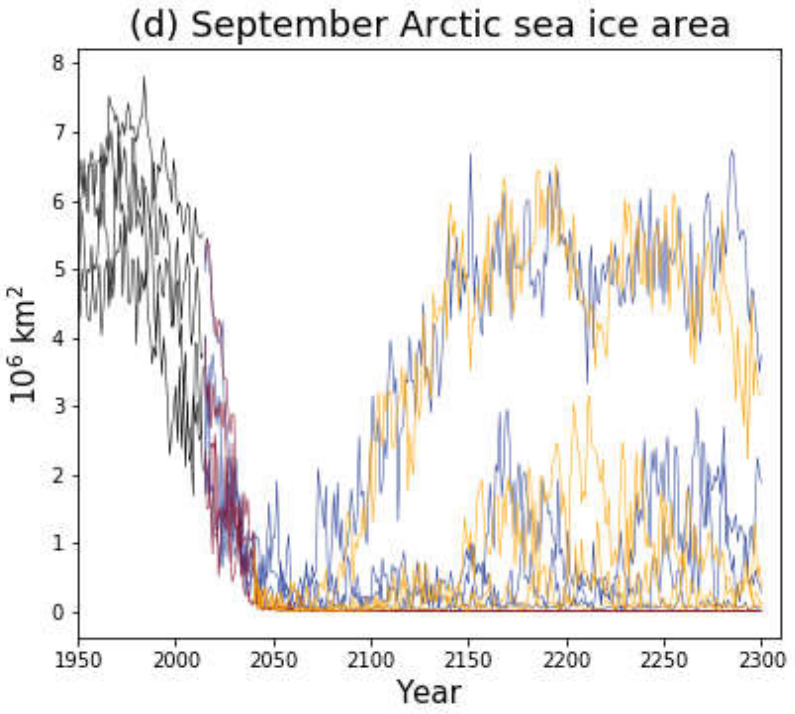

IPCC 2021, Chap. 4

Chapter 5: Global Carbon and other Biogeochemical Cycles and Feedbacks